厚生労働科学研究費補助金

萌芽的先端医療技術推進研究事業

ナノレベルイメージングによる分子の機能および構造解析に関する研究（H14-ナノ-001）

平成14-18年度　総合研究報告書

Vol.3

主任研究者　盛　英三

平成19年（2007年）3月

articles

Structure of the core domain of human cardiac troponin in the Ca^{2+}-saturated form

Soichi Takeda*†‡, Atsuko Yamashita*, Kayo Maeda* & Yuichiro Maéda*

** Laboratory for Structural Biochemistry, RIKEN Harima Institute at SPring-8, 1-1-1 Kouto, Mikazuki, Sayo, Hyogo 679-5148, Japan*
† PRESTO, Japan Science and Technology Corporation (JST), Kawaguchi, Saitama 332-0012, Japan

Troponin is essential in Ca^{2+} regulation of skeletal and cardiac muscle contraction. It consists of three subunits (TnT, TnC and TnI) and, together with tropomyosin, is located on the actin filament. Here we present crystal structures of the core domains (relative molecular mass of 46,000 and 52,000) of human cardiac troponin in the Ca^{2+}-saturated form. Analysis of the four-molecule structures reveals that the core domain is further divided into structurally distinct subdomains that are connected by flexible linkers, making the entire molecule highly flexible. The α-helical coiled-coil formed between TnT and TnI is integrated in a rigid and asymmetric structure (about 80 Å long), the IT arm, which bridges putative tropomyosin-anchoring regions. The structures of the troponin ternary complex imply that Ca^{2+} binding to the regulatory site of TnC removes the carboxy-terminal portion of TnI from actin, thereby altering the mobility and/or flexibility of troponin and tropomyosin on the actin filament.

In muscle contraction, generation of force is coupled with ATPase and is exerted by the interaction between myosin subfragment 1 and the actin-containing muscle thin filament. In skeletal and cardiac muscle, contraction is regulated by intracellular Ca^{2+} concentration. The molecular basis for Ca^{2+} regulation was first established by Ebashi and co-workers in the 1960s, where they identified troponin and tropomyosin as the principal proteins of Ca^{2+} regulation[1]. Troponin (relative molecular mass of approximately 80,000 (80K)) and tropomyosin are generally located along polymerized actin, which forms the backbone of the filament, at a troponin:tropomyosin:actin ratio of 1:1:7 (ref. 2). Troponin consists of three subunits: TnC, the Ca^{2+}-binding subunit; TnI, the inhibitory subunit; and TnT, the tropomyosin-binding subunit[3–5]. Tropomyosin is a α-helical coiled-coil protein throughout its entire length, and interacts with adjacent tropomyosin molecules in a head-to-tail manner, forming continuous strands that lie along the thin filament[6].

The crystal structure of TnC in complex with the amino-terminal segment of TnI provided insight into the mechanism of calcium regulation[7]. TnC consists of two globular lobes[8,9] connected by a flexible linker[10]. In muscle cells, the C lobe is believed to be continuously occupied with metal ions[4], and it opens up the hydrophobic patch to bind the N-terminal amphiphilic α-helix of TnI (the first TnC-binding site), which anchors TnC to the rest of troponin, and thus has a structural role[7,11]. At low Ca^{2+} concentrations, the inhibitory region (residues 137–148 in human cardiac TnI) interacts with actin, and thereby inhibits actomyosin ATPase[12–14]. On the basis of the structural details of binding in the C lobe, together with the calcium-saturated TnC structure[10], the same manner of interactions in the N lobe was proposed[7]—with an increase in intracellular Ca^{2+} concentration, Ca^{2+} binding to the N lobe would open up the hydrophobic patch to bind to the second amphiphilic α-helix of TnI, which is immediately downstream of the inhibitory region. The inhibitory region is then detached from actin-tropomyosin, resulting in the release of inhibition. The interaction between the N lobe and the TnI amphiphilic segment was confirmed by an NMR study[15].

Although there is little doubt that the changes in the interactions between TnC and TnI have primary roles in the onset of muscle contraction, the mechanism by which troponin–tropomyosin regulates the actomyosin ATPase has remained elusive. This is because high-resolution structures have been available for only a small portion of the troponin–tropomyosin–actin complex. Electron microscopy[16–18] and low-resolution X-ray crystallography[19] studies have revealed that troponin consists of two domains: the TnT1 extension and the rest of troponin, referred to as the core domain. We have chosen the core domain for the target of crystallographic study, as this retains most of the regulatory function of troponin[20]. Here we describe the crystal structure of two kinds of core domain of human cardiac troponin in the Ca^{2+}-saturated form; one at 2.6 Å resolution and the other at 3.3 Å resolution. These crystal structures elucidate how three polypeptide chains are folded around each other within the troponin molecule.

Structure determination

We crystallized two distinct preparations of the troponin core domain, which were reconstituted from *Escherichia coli*-expressed recombinant human cardiac troponin subunits. One core domain had a relative molecular mass of 46K (Tn46K), consisting of TnC(1–161), TnI(31–163) and TnT(183–288), whereas the other was 52K (Tn52K), consisting of TnC(1–161), TnI(31–210) and TnT(183–288). Our crystallization trials of the entire troponin molecule were not successful, presumably due to the association of the extended structure of TnT1, which must have an extended binding site to tropomyosin[17–19,21]. Both crystal forms grew in the presence of Ca^{2+}, so that all of the metal-binding sites were occupied (Ca^{2+}-bound form). In both cases, the cardiac-specific sequence (TnI residues 1–30) was removed, which makes each subunit almost identical to the skeletal muscle troponin counterpart. In Tn46K, but not in Tn52K, an extra 46 residues were deleted from the C terminus of TnI, because the deletion improved the crystal quality. However, this deletion is known to impair the ability of TnI to bind to actin–tropomyosin at low Ca^{2+} concentrations[20].

The Tn46K structure was determined by the multi-wavelength anomalous dispersion (MAD) method, and was refined against the native crystal data up to 2.6 Å to an *R*-factor of 25.9% (R_{free} 29.7%). The Tn52K structure was determined by molecular replacement

‡ Present address: Department of Cardiac Physiology, National Cardiovascular Center Research Institute, 5-7-1 Fujishiro-dai, Suita, Osaka 565-8565, Japan.

using the Tn46K structure and was refined up to 3.3 Å resolution to an *R*-factor of 25.1% (R_{free} 30.8%) (Table 1). The asymmetric unit of each crystal form contained two troponin molecules, and thus we obtained the structures of four molecules in total, which we term Tn46KA, Tn46KB, Tn52KA and Tn52KB.

Overall architecture and subunit arrangement

The overall architecture of the Tn52KB molecule is shown in Fig. 1a. Notably, the core domain is dominated by α-helices. The core domain is further divided into two structurally distinct subdomains (Fig. 1b), denoted as the regulatory head (consisting of TnC residues 3–84 and TnI residues 150–159) and the IT arm (consisting of TnC residues 93–161, TnI residues 42–136 and TnT residues 203–271). All four molecules are similar to each other, except for the relative orientation between the two subdomains (see below).

Each lobe of TnC superposes almost exactly onto its counterpart in the previously reported TnC–TnI binary complexes: Protein Data Bank code 1MXL[15] (the root mean square (r.m.s.) deviation between the equivalent Cα atoms in the TnC N lobe is 1.50 Å) and 1A2X[7] (the r.m.s. deviation in the TnC C lobe is 1.04 Å).

The N terminus of TnI (residues 31–34) was not well defined in either molecule, and the following residues 35–42 are highly variable among the four molecules. Residues 43–79 form the α-helix, H1(I), and its amphiphilic portion (residues 43–65) binds to the C lobe of TnC through multiple polar and van der Waals interactions (the first TnC-binding site in TnI), as already shown in the TnC–TnI(1–47) binary complex[7]. The C-terminal portion of H1(I) (residues 66–79), which was disordered in the binary complex crystal[7], is stabilized here by interacting with TnT through multiple hydrogen bonds as well as hydrophobic interactions (Fig. 1c). TnI residues 80–89, which are less conserved and contain two glycines and one proline, have an extended structure and interact with TnT, forming a hydrophobic core (Fig. 1c; Leu 83, Leu 85, Leu 88, Leu 93 and Leu 96 of TnI, and Ala 233, Arg 230 and Leu 229 of TnT are involved in the interaction).

The H2(I) helix (TnI residues 90–135) forms a parallel α-helical coiled-coil with the H2(T2) helix (residues 226–271) of TnT (Fig. 1), as previously suggested[22,23]. Each chain has 6.5 heptad repeats, with hydrophobic residues at the a and d positions (see Supplementary Fig. 1). The amino acid residues involved in the inter-chain interactions are well conserved even in invertebrate species (see Supplementary Fig. 1), suggesting that this coiled-coil between TnT and TnI has important physiological roles that are characteristic of troponin. At the C terminus of the coiled-coil, TnT (residues 256–270) interacts with TnC (see below).

Downstream from the coiled-coil is the TnI inhibitory region (residues 137–148). In the present structures, the electron densities associated with the inhibitory region were not well defined in either molecule. However, the inhibitory region must be extended judging from the Cα distances (26.2–32.6 Å, depending on the four molecules) between Arg 136 and Thr 149, spanning 13 residues. The inhibitory region is followed by another amphiphilic α-helix, H3(I), which spans residues 150–159 of TnI, and interacts with the hydrophobic cleft of the N lobe of TnC through multiple van der Waals contacts (the second TnC-binding site in TnI; see below). Further downstream of H3(I), residues 164–188 form a protruded α-helix, H4(I), that has no direct interaction with the rest of the molecule (Fig. 1a, b). H4(I) was clearly defined in only one molecule (Tn52KB) within an asymmetric unit, and was probably stabilized through eventual molecular contacts with the loop between H1(I) and H2(I) of the symmetry-related molecule. On the other hand, Tn52KA lacks a defined protruded α-helix, but has a loop (residues 160–162) pointing in a different direction than that of Tn52KB (Fig. 2a), owing to a kink at Gly 160. Although we found further extended electron densities of TnI in the Tn52KA molecule in this direction, they were quite ambiguous, so we did not include these residues in the model. TnI residues 189–191 of Tn52KB are in an extended structure that eventually interacts with the next molecule, whereas the electron density associated with the C terminus (residues 192–210) was not defined. The C terminus of TnT (denoted as C-TnT, residues 272–288), which has been shown to bind to tropomyosin[24–26], is not always defined in the crystal (the residues down to 276 are defined in Tn52KB). Upstream from the coiled-coil, residues 204–220 of TnT form another α-helix, H1(T2), which is kinked by about 60° relative to H2(T2) (Fig. 1a, c). H1(T2) is predominantly stabilized against the rest of the molecule through two sets of hydrogen bonds: one is between Glu 214 of TnT and Arg 98 of TnI, and the other is between Arg 216 of TnT and Asp 105 of TnI in Tn46KA (Fig. 1c) and in Tn52KA (not shown). However, Tn46KB and Tn52KB lack these hydrogen bonds, probably due to the distinct molecular packing in the crystal lattice (data not shown). Further upstream of H1(T2), residues 183–202 of TnT were not defined in the electron density map.

As described above, most of the electron densities associated with the potential actin–tropomyosin interfaces are ambiguous. These include the inhibitory region (residues 137–148) and the C-terminus of TnI (residues 163–210 in Tn52KA and 192–210 in Tn52KB), and the C-TnT (residues 272–288). In total, 12.5% of the Tn46K and 19.4% of the Tn52K amino acid residues are not included in the current models. These regions lack direct interactions with the remainder of the molecule and are susceptible to proteases[20,24]. It is therefore plausible that these actin–tropomyosin-binding sites may not properly fold in solution, or alternatively, that these regions may contain flexible linkers that allow multiple conformations. The structures from the two crystal forms show relatively high overall *B*-factors (the averaged *B*-factors are 73.0 Å^2 for Tn46K and 91.7 Å^2 for Tn52K), consistent with the rapid decrease of the diffraction intensities in the higher angle region. The high *B*-factors are probably derived from the extremely high flexibility of the molecule at the subdomain junction (see below). The high overall *B*-factors, together with the substantial extension of the disordered regions, might contribute to the relatively high *R*-factors. However, the experimentally phased electron density maps (data not shown) and the final $2F_o–F_c$ map (Fig. 1d, e) seemed to be of sufficient quality for the structural determination. The unusual flexibility is a remarkable characteristic of the troponin molecule. As troponin is quite flexible, the molecule is able to evade packing in a crystalline lattice for a long time.

Table 1 **Refinement statistics**

	Core domains	
	Tn46K	Tn52K
Resolution (Å)	40.0–2.61	20.0–3.30
Reflections	27,881	16,015
R^*	0.264	0.251
R_{free}^*	0.298	0.308
Number of atoms		
Protein	5,673	5,858
Water	102	0
Calcium ion	6	6
Average *B* (Å^2)	73.0	91.7
Ramachandran plot		
Most favoured/allowed (%)	91.8/8.2	91.5/8.5
r.m.s. deviations		
Bond length (Å)/bond angle (°)	0.0085/1.398	0.0089/1.40

*$R = \Sigma||F_o| - |F_c||/\Sigma|F_o|$. R_{free} is the R value for a subset of 5% of the reflection data, which were not included in the crystallographic refinement.

Flexible linkers between the two subdomains

In Fig. 2, the four molecules are superposed, with a fixed orientation of either the regulatory head (Fig. 2a) or the IT arm (Fig. 2b). The r.m.s. deviations between all of the equivalent Cα atoms of any two of the four troponin molecules are 0.52–0.81 Å for the regulatory head and 0.68–1.70 Å for the IT arm. Except for the loop (TnI residues 81–89) in Tn52KB, the atomic coordinates within each

subdomain are almost identical among the four molecules, indicating that each subdomain behaves as a unit. On the other hand, the relative orientation between the two subdomains is quite variable among the four molecules. The largest difference exists between Tn46KA and Tn46KB, where the IT arm should be rotated by 20° relative to the regulatory head subdomain, bringing about a 27 Å displacement at the distal end of the IT arm (Fig. 2a).

On the basis of this observation and the following considerations, we suggest that the linker between the two subdomains works as a universal joint. First, the unique covalent link between the two subdomains—that is, the linker connecting the two lobes of TnC (D/E-linker)—must be highly mobile. The relative orientation between the two lobes in our structures is completely different from those reported previously[7–9,27] (Fig. 3). In our study, the D/E-linker in each molecule is not clearly defined owing to the lack of specific interactions with the rest of the molecule. TnC mutants

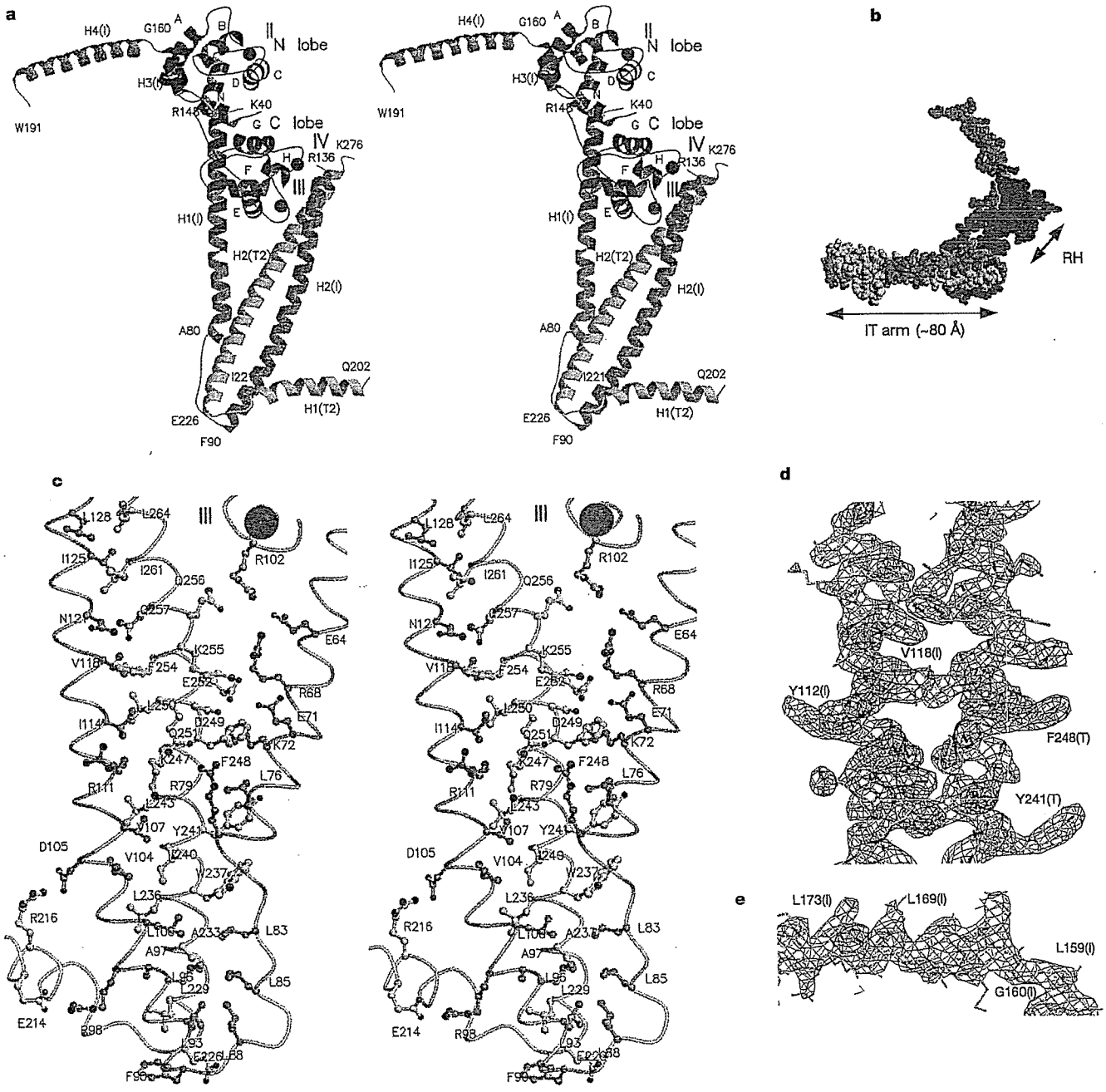

Figure 1 Crystal structure of the troponin core domain. **a**, Stereo view of the Tn52KB molecule. TnC and TnT are coloured in red and yellow, respectively. TnI is coloured in cyan, except for the two stretches of amphiphilic helices (TnC-binding sites), which are dark blue. The three Ca^{2+} ions bound to the Ca^{2+}-binding sites (II–IV) are represented by black spheres. Each helix within TnI and TnT is indicated by the helix number, whereas each helix of TnC is indicated by a capital letter (N and A–H). **b**, A space-filling model of the Tn52KB molecule. RH, regulatory head. **c**, A close-up stereo view of the IT-arm portion (Tn46KA), viewed from the other side of **a**. **d**, $2F_o$–F_c electron density map (1.5σ contoured) associated with the middle region of the coiled-coil at 2.6 Å resolution (Tn46KA). **e**, $2F_o$–F_c map (1.2σ contoured) associated with the protruded helix, H4(I), at 3.3 Å resolution (Tn52KB). Figures 1–5 were generated by TURBO-FRODO[46], MOLSCRIPT[49] and Raster3D[50].

with D/E-linker deletions do not show a significant impairment in regulatory activity, whereas mutants that reduce the flexibility of the D/E-linker impair the ability to activate the thin filament[28,29]. Thus, the flexibility, not the length (which would specify the relative orientation between the two lobes), of the D/E-linker is crucial for the activity of troponin. Second, the direct contacts between the regulatory head and the IT arm are mediated by a small number of residues (data not shown) that are poorly conserved among species, and therefore the contact may not be specific, but would eventually be stabilized by the crystal-packing force. Third, the link through TnI, the inhibitory region that connects H2(I) and H3(I), is not well defined in the present structures, indicating that this link is also flexible. Altogether, these findings indicate that the troponin molecule might adopt multiple conformations with variable subdomain orientations when it is located on the filament, as well as within the crystal.

Integration of the C lobe of TnC

At the C terminus of the coiled-coil, TnT interacts with the C lobe of TnC (Fig. 4a). Therefore, all three polypeptide chains of troponin come together in this region to interact in a specific manner. Here, helix H2(T2) interacts with TnI by forming a coiled-coil on one side. The other side of H2(T2) interacts with the Ca^{2+}-binding loops of TnC: TnT residues Tyr 259, Val 263, Asn 266, Arg 267 and Asp 270 interact with TnC residues Phe 101, Arg 102, Asp 105, Asp 109 and Tyr 111 within loop III, and with Asp 149, Tyr 150 and Asp 151 within loop IV. Notably, Asp 270 of TnT forms a hydrogen bond with the hydroxyl group of Tyr 111 of TnC, which simultaneously coordinates the calcium ion in site III with its carbonyl oxygen. Moreover, although the side chain of Asp 109 is also involved in calcium binding, its carbonyl oxygen also forms a hydrogen bond with Asn 266 of TnT. These findings suggest that the binding of Ca^{2+} ions to the C lobe is required not only to keep the C lobe tightly folded to bind to the amphiphilic helix of TnI (the first TnC-binding site in TnI), but also to stabilize the interaction between TnC and TnT. As the metal-binding sites in the C lobe (site III and IV) are believed to be occupied with either Ca^{2+} or Mg^{2+} ions *in vivo*, irrespective of the sarcoplasmic Ca^{2+} concentration[4], the C lobe is rigidly integrated in the IT arm, and this structure remains unchanged and is independent of the physiological states of the thin filament. It is worth noting that the integration site of three chains resides immediately upstream of the C-terminal region of TnT (C-TnT, residues 272–288) through which the structure is anchored to actin–tropomyosin[24–26], and the C-terminal region of TnI (TnI_{reg}, residues 137–210), which must undergo major conformational changes depending on the Ca^{2+} concentration (see below).

Molecular switch

There is little doubt that the amphiphilic helix H3(I) works as a molecular switch that transmits the initial signal of Ca^{2+} binding to the N lobe of TnC to the other components in the thin filament, and thus has a central role in the initial steps of troponin–tropomyosin-based regulation. As discussed previously[7], amphiphilic helix H3(I) binds specifically to the hydrophobic patch of the Ca^{2+}-saturated N lobe of TnC (Fig. 4b) through conserved hydrophobic residues (Supplementary Fig. 1b), and the interactions are Ca^{2+}-dependent[15,20]. The segment H3(I) is located in the sequence between the two putative actin-binding sites, the inhibitory region (residues 137–148) and the C terminus of TnI (residues 169–210)[20], which were both shown to be essential for the inhibitory binding of TnI in the absence of Ca^{2+} (ref. 14) and to change the distances to the nearby actin molecule depending on the Ca^{2+} concentrations[30,31]. Residues 167–184 are highly conserved (Supplementary Fig. 1b) and form the amphiphilic helix, H4(I); the corresponding peptide (residues 128–148 in skeletal TnI) binds to actin–tropomyosin and induces a weak inhibitory activity on its own[32]. Finally, in the presence of Ca^{2+}, TnI is released from its binding site on actin-tropomyosin[33]. Therefore, the binding of H3(I) to the hydrophobic patch of the N lobe of TnC must induce the detachment of the substantially extended C-terminal portion of TnI, denoted as the regulatory segment of TnI, TnI_{reg} (residues 137–210), from the actin filament.

Interactions of troponin and other thin filament components

Troponin is anchored to the thin filament mainly through tropomyosin binding of two distinct portions of TnT; that is, TnT1 and C-TnT[16,24–26]. The former is believed to be the major Ca^{2+}-insensitive anchoring site of troponin onto tropomyosin, whereas the interaction through the latter is stronger at low, rather than high, Ca^{2+} concentrations[25] (Fig. 5). No part of the IT arm is known to have direct interactions with actin or with tropomyosin. On the basis of the present structures, the separation between TnT1 and C-TnT is estimated to be about 60 Å (Fig. 5), although these two portions are not included in the current crystal structures. TnT1 has a high α-helical content and is less susceptible to proteolysis, indicating that it forms another structural domain[16,19]. TnT residues 183–200 probably work as a flexible linker between the two subdomains, TnT1 and the IT arm. This segment is not defined in

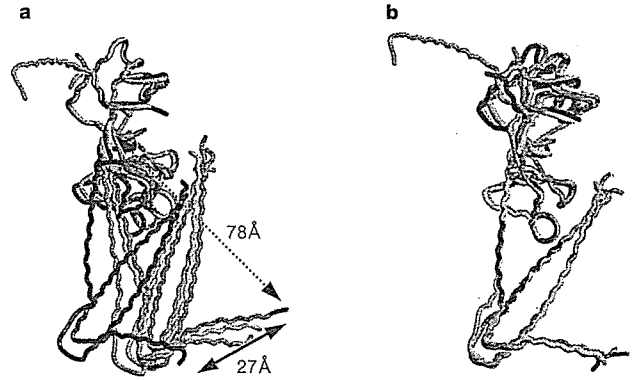

Figure 2 Comparison of the four troponin core domain molecules from two crystal forms, Tn46K and Tn52K. The four molecules are superposed, with the best superposition (the least square fit) of either the regulatory head (**a**) or the IT arm (**b**). The molecules Tn46KA, Tn46KB, Tn52KA and Tn52KB are coloured red, cyan, yellow, and light pink, respectively.

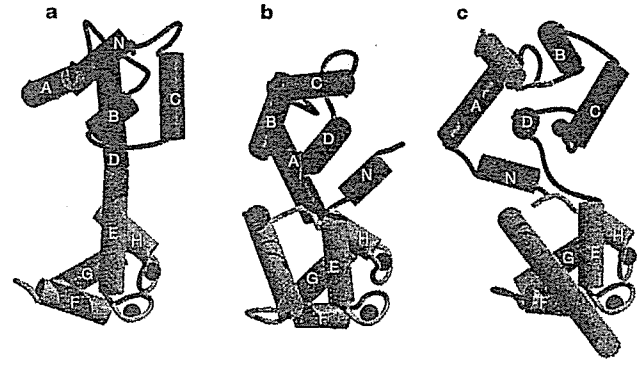

Figure 3 Comparison of the TnC conformations, represented by cylinders (α-helices) and wires (loops). **a**, Crystal structure of TnC alone (Protein Data Bank code 1TOP[9]); **b**, TnC in complex with the N-terminal fragment of TnI (1A2X[7]); and **c**, TnC in the present study (Tn46KA). The C lobes are aligned in almost the same orientation. The N and C lobes are red and orange, respectively, whereas the bound TnI segments are cyan. Bound calcium ions are represented by black spheres. The TnC helices, N and A–H, are indicated.

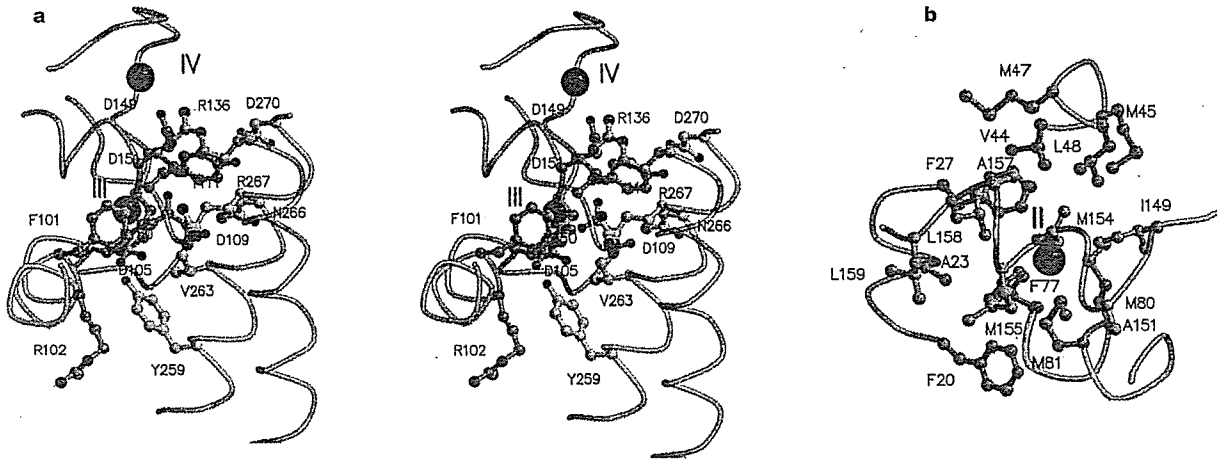

Figure 4 Side-chain interactions between the subunits. **a**, A stereo view of the interactions between the three chains around the C lobe of TnC. **b**, The hydrophobic residues in the N lobe of TnC interacting with segment H3(I) of TnI. TnC, TnI and TnT are coloured pink, cyan and yellow, respectively. The amino acid residues involved in the interactions are shown in ball and stick representation. The three Ca^{2+} ions bound to sites II, III and IV are shown by the black spheres.

the present structures, is less conserved (Supplementary Fig. 1a) and is susceptible to proteolysis[16,26].

At a low Ca^{2+} concentration, the N lobe of TnC dissociates H3(I). It has been interpreted that TnI should form another attachment to the filament, most probably to create the ternary complex actin–tropomyosin–TnI[32,33], whereas others have shown that TnI cross-links only to actin[30].

Discussion

The present structures have elucidated the overall architecture of the troponin molecule. Troponin appears to be divided into subdomains, including the regulatory head, the IT arm, TnT1, C-TnT and TnI_{reg}. The subdomains are defined by boundaries that do not coincide at all with the boundaries of the three polypeptide chains. The subdomains are connected by flexible linkers, making the entire molecule quite flexible. The flexible nature of the troponin molecule must be relevant to the physiological function. Although many residues are left unidentified in the present electron density maps and some residues are quite variable among the four molecules, the atomic positions in the remaining parts are reliable, partly because the structure has been solved four times. Actually, the missing residues and the differentiated relative orientations of individual subdomains among four molecules indicate that the linkers are flexible. The characteristic architecture implies that molecular motions of troponin could be described in terms of changes of orientation of individual α-helices plus mobility of individual flexible linkers.

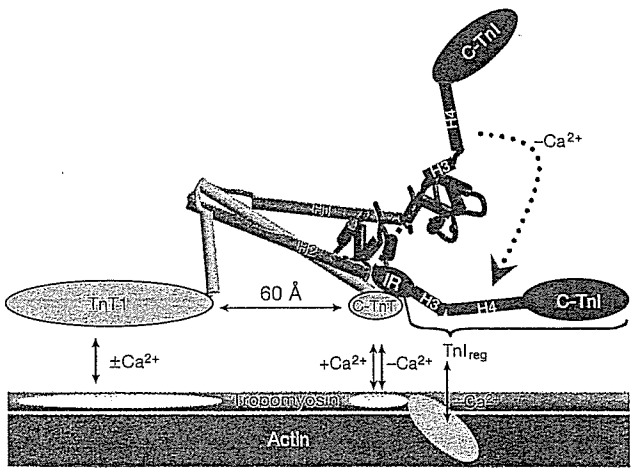

Figure 5 A schematic representation of the interactions between troponin and other thin filament components. The potential actin–tropomyosin-binding portions, which are not included in the current structural model, are schematically drawn: TnT1 and C-TnT are yellow ellipsoids, and the inhibitory region (IR) and the C terminus of TnI (C-TnI) are blue ellipsoids. The actin and the tropomyosin strands are in green and brown, respectively. The black arrows indicate the interactions between troponin and tropomyosin–actin.

During calcium regulation, TnI_{reg} must undergo major changes both in position and conformation. At higher Ca^{2+} concentrations, TnI_{reg} is detached from actin–tropomyosin, being associated with the N lobe of TnC in an extended form as shown in the present structures. At lower Ca^{2+} concentrations, TnI_{reg} must form an extra attachment to actin–tropomyosin so that the troponin–tropomyosin strand is tied down onto the actin filament. Within the extra attachment, the entire TnI_{reg} might be folded, as complete inhibition requires an extended region, at least residues spanning 185–210 (refs 14, 20), and as the space available on actin–tropomyosin might be limited if TnI_{reg} binds to one of the seven actin monomers.

The IT arm must also have an important function in calcium regulation. This subdomain is large and rigid, being conserved between species and having no direct interaction with actin–tropomyosin. Its location is remarkable—this structure bridges the two (largely) Ca^{2+}-independent attachments to actin–tropomyosin, TnT1 and C-TnT. Moreover, the IT arm resides immediately upstream, not only from the tropomyosin-binding site (C-TnT) but also from the mobile TnI_{reg} that changes position and conformation in a Ca^{2+}-dependent manner, promoting the transition from two points of attachment to three points of attachment of troponin to actin–tropomyosin. An intriguing possibility is that the formation of the third attachment (by TnI_{reg}) could cause a minute rotation of the IT arm about the pivotal point; that is, the C-terminal end of the coiled-coil. The formation of the third attachment itself, as well as the rotation of the IT arm, might change the properties of the tropomyosin strand on the actin filament.

The nature of the changes remain unknown. Although many previous results have been interpreted to be consistent with the proposal[34–36] for the shift in azimuthal position of the tropomyosin strands, the systematic FRET experiments[37] consistently failed to provide evidence of any major change in the distance between tropomyosin and actin. A more plausible explanation is that the strain imposed on the tropomyosin strand is altered; thereby the

mobility and/or the flexibility of the tropomyosin strand might be changed[38]. Being consistent with this view, the atomic model of the actin–tropomyosin complex (without troponin)[39] indicated that the tropomyosin strand 'diffuses' around actin, being weakly held by electrostatic forces. Further investigations are required to elucidate the structure of the troponin–tropomyosin complex corresponding to each state in the three-state model[40]. In this context, it is worth noting that the thin-filament-associated X-ray diffraction intensities as well as electron micrographs have been interpreted based on the assumption that the mass of the troponin–tropomyosin complex is distributed evenly and smoothly all through the continuous 'tropomyosin strands'. With the present atomic structures, trials are now underway to identify separately the mass of tropomyosin and that of troponin on the muscle thin filament. □

Methods

Protein preparations

Details about the construction of the expression vectors and the sample preparation will be described elsewhere. We prepared individual subunits of human cardiac troponin separately in *E. coli*. TnT2 (residues 183–288) was prepared by chemical cleavage. First, TnT(25K)[41] (TnT residues 94–288) was expressed and purified. Then TnT(25K) was further cleaved by cyanogen bromide to obtain TnT2, which was purified by reverse phase high-performance liquid chromatography (HPLC) followed by size exclusion chromatography. As previously demonstrated for the TnI(1–47) fragment[7], when preparing peptide fragments, the chemical cleavage method gives rise to more homogenous and stable preparations that lack proteolytic activity as compared with limited proteolysis or direct expression of the fragment in *E. coli*. For TnC, the cysteine-less variant TnC(C35S/C84S) was used. For TnI, the variants (T31M/C80A/C97A) were used, which each start from Met 31. The ternary complexes were prepared[20] with minor modifications. For preparing the strontium-substituted Tn46K crystals, $SrCl_2$ instead of $CaCl_2$ was added to the solutions throughout the purification procedure. The final protein solutions contained 10 mM Tris-HCl, 150 mM NaCl and either 0.1 mM $CaCl_2$ or 0.1 mM $SrCl_2$ at pH 8.

Crystallization

Native and strontium-substituted crystals were grown using the hanging-drop vapour diffusion technique, with reservoir solutions containing 20% PEG3350, 15% glycerol, 0.1 M LiCl, 50 mM Tris-HCl and either 5 mM $CaCl_2$ or 5 mM $SrCl_2$ at pH 8. Drops composed of 2 μl of protein at 10 mg ml^{-1} and 2 μl of the reservoir solution were equilibrated with 0.5 ml of reservoir solution for a minimum of two weeks at 20 °C. Tn46K and Tn52K crystallized in space group $P2_1$ with unit cell dimensions of $a = 42.3$ Å, $b = 167.9$ Å, $c = 69.7$ Å, $\beta = 101.4°$ and $a = 48.3$ Å, $b = 169.5$ Å, $c = 68.5$ Å, $\beta = 102.4°$, respectively. The osmium-derivative crystal was prepared by soaking the native Tn46K crystal in a reservoir solution supplemented with 1 mM $OsCl_3$ for 18 h. The crystals were flash frozen under a nitrogen flow at 100K after the glycerol concentration was increased to 20% by soaking.

Diffraction data collection and structural analysis

All diffraction data were collected at SPring-8 (beam lines BL41XU, BL44B2 and BL45XU) using either Mar CCD (charge-coupled device) 165 or Rigaku R-AXIS V detectors at 90K. The images were reduced using HKL2000 (ref. 42). The initial phases were obtained at 3.3 Å resolution by the MAD method, using an osmium derivative data set. The heavy atom positions were searched for by SOLVE[43], and the phases were calculated using SHARP[44] and further improved by SOLMON[45]. Model building was carried out using TURBO-FRODO[46]. Although the Os MAD map enabled us to trace almost the entirety of the chains, the quality of the map was not sufficient to complete the model building in detail. Then, we obtained new phases to 2.8 Å resolution using a set of MAD data from a strontium-substituted crystal, which enabled us to complete the model building. In the crystal, six Sr^{2+} ions were coordinated in the Ca^{2+}-binding sites (II–IV). The structural models (Protein Data Bank codes 1MXL[15] and 1A2X[7]) were used as guides for the model building. The model was refined against the native Tn46K data set to 2.6 Å resolution using CNS[47] (including the bulk solvent correction, the simulated annealing, the minimization and the individual *B*-factor refinements), and the subsequent rounds of model building and refinement produced the final structural model for two Tn46K molecules.

The structure of Tn52K was solved by molecular replacement, using the refined Tn46K model. To do this, the Tn46K subdomains, the IT arm and regulatory head were separately used as the search models by the program MOLREP in the CCP4 suite[48]. The subsequent rounds of model building and refinement (as described above plus the grouped-*B*-factor refinement) produced the final structural model for the two Tn52K molecules.

Received 24 December 2002; accepted 28 April 2003; doi:10.1038/nature01780.

1. Ebashi, S. & Endo, M. Calcium ion and muscle contraction. *Prog. Biophys. Mol. Biol.* 18, 123–183 (1968).
2. Ebashi, S., Endo, M. & Otsuki, I. Control of muscle contraction. *Q. Rev. Biophys.* 2, 351–384 (1969).
3. Ohtsuki, I., Maruyama, K. & Ebashi, S. Regulatory and cytoskeletal proteins of vertebrate skeletal muscle. *Adv. Protein Chem.* 38, 1–67 (1986).
4. Zot, A. S. & Potter, J. D. Structural aspects of troponin–tropomyosin regulation of skeletal muscle contraction. *Annu. Rev. Biophys. Biophys. Chem.* 16, 535–559 (1987).
5. Farah, C. S. & Reinach, F. C. The troponin complex and regulation of muscle contraction. *FASEB J.* 9, 755–767 (1995).
6. Phillips, G. N. Jr, Fillers, J. P. & Cohen, C. Tropomyosin crystal structure and muscle regulation. *J. Mol. Biol.* 192, 111–131 (1986).
7. Vassylyev, D. G., Takeda, S., Wakatsuki, S., Maeda, K. & Maéda, Y. Crystal structure of troponin C in complex with troponin I fragment at 2.3-Å resolution. *Proc. Natl Acad. Sci. USA* 95, 4847–4852 (1998).
8. Herzberg, O. & James, M. N. Structure of the calcium regulatory muscle protein troponin-C at 2.8 Å resolution. *Nature* 313, 653–659 (1985).
9. Sundaralingam, M. *et al.* Molecular structure of troponin C from chicken skeletal muscle at 3-angstrom resolution. *Science* 227, 945–948 (1985).
10. Slupsky, C. M. & Sykes, B. D. NMR solution structure of calcium-saturated skeletal muscle troponin C. *Biochemistry* 34, 15953–15964 (1995).
11. Gasmi-Seabrook, G. M. *et al.* Solution structures of the C-terminal domain of cardiac troponin C free and bound to the N-terminal domain of cardiac troponin I. *Biochemistry* 38, 8313–8322 (1999).
12. Syska, H., Wilkinson, J. M., Grand, R. J. & Perry, S. V. The relationship between biological activity and primary structure of troponin I from white skeletal muscle of the rabbit. *Biochem. J.* 153, 375–387 (1976).
13. Talbot, J. A. & Hodges, R. S. Synthetic studies on the inhibitory region of rabbit skeletal troponin I. Relationship of amino acid sequence to biological activity. *J. Biol. Chem.* 256, 2798–2802 (1981).
14. Farah, C. S. *et al.* Structural and regulatory functions of the NH2- and COOH-terminal regions of skeletal muscle troponin I. *J. Biol. Chem.* 269, 5230–5240 (1994).
15. Li, M. X., Spyracopoulos, L. & Sykes, B. D. Binding of cardiac troponin-I147-163 induces a structural opening in human cardiac troponin-C. *Biochemistry* 38, 8289–8298 (1999).
16. Ohtsuki, I. Molecular arrangement of troponin-T in the thin filament. *J. Biochem. (Tokyo)* 86, 491–497 (1979).
17. Flicker, P. F., Phillips, G. N. Jr & Cohen, C. Troponin and its interactions with tropomyosin. An electron microscope study. *J. Mol. Biol.* 162, 495–501 (1982).
18. Ohtsuki, I., Onoyama, Y. & Shiraishi, F. Electron microscopic study of troponin. *J. Biochem. (Tokyo)* 103, 913–919 (1988).
19. White, S. P., Cohen, C. & Phillips, G. N. Jr Structure of co-crystals of tropomyosin and troponin. *Nature* 325, 826–828 (1987).
20. Takeda, S., Kobayashi, T., Taniguchi, H., Hayashi, H. & Maeda, Y. Structural and functional domains of the troponin complex revealed by limited digestion. *Eur. J. Biochem.* 246, 611–617 (1997).
21. Schaertl, S., Lehrer, S. S. & Geeves, M. A. Separation and characterization of the two functional regions of troponin involved in muscle thin filament regulation. *Biochemistry* 34, 15890–15894 (1995).
22. Pearlstone, J. R. & Smillie, L. B. The interaction of rabbit skeletal muscle troponin-T fragments with troponin-I. *Can. J. Biochem. Cell Biol.* 63, 212–218 (1985).
23. Stefancsik, R., Jha, P. K. & Sarkar, S. Identification and mutagenesis of a highly conserved domain in troponin T responsible for troponin I binding: potential role for coiled coil interaction. *Proc. Natl Acad. Sci. USA* 95, 957–962 (1998).
24. Tanokura, M., Tawada, Y., Ono, A. & Ohtsuki, I. Chymotryptic subfragments of troponin T from rabbit skeletal muscle. Interaction with tropomyosin, troponin I and troponin. *C. J. Biochem. (Tokyo)* 93, 331–337 (1983).
25. Pearlstone, J. R. & Smillie, L. B. Effects of troponin-I plus-C on the binding of troponin-T and its fragments to alpha-tropomyosin. Ca^{2+} sensitivity and cooperativity. *J. Biol. Chem.* 258, 2534–2542 (1983).
26. Morris, E. P. & Lehrer, S. S. Troponin-tropomyosin interactions. Fluorescence studies of the binding of troponin, troponin T, and chymotryptic troponin T fragments to specifically labeled tropomyosin. *Biochemistry* 23, 2214–2220 (1984).
27. Houdusse, A., Love, M. L., Dominguez, R., Grabarek, Z. & Cohen, C. Structures of four Ca^{2+}-bound troponin C at 2.0 Å resolution: further insights into the Ca^{2+}-switch in the calmodulin superfamily. *Structure* 5, 1695–1711 (1997).
28. Ramakrishnan, S. & Hitchcock-DeGregori, S. E. Investigation of the structural requirements of the troponin C central helix for function. *Biochemistry* 34, 16789–16796 (1995).
29. Babu, A., Rao, V. G., Su, H. & Gulati, J. Critical minimum length of the central helix in troponin C for the Ca^{2+} switch in muscular contraction. *J. Biol. Chem.* 268, 19232–19238 (1993).
30. Luo, Y. *et al.* Photocrosslinking of benzophenone-labeled single cysteine troponin I mutants to other thin filament proteins. *J. Mol. Biol.* 296, 899–910 (2000).
31. Li, Z., Gergely, J. & Tao, T. Proximity relationships between residue 117 of rabbit skeletal troponin-I and residues in troponin-C and actin. *Biophys. J.* 81, 321–333 (2001).
32. Tripet, B., Van Eyk, J. E. & Hodges, R. S. Mapping of a second actin-tropomyosin and a second troponin C binding site within the C terminus of troponin I, and their importance in the Ca^{2+}-dependent regulation of muscle contraction. *J. Mol. Biol.* 271, 728–750 (1997).
33. Geeves, M. A., Chai, M. & Lehrer, S. S. Inhibition of actin-myosin subfragment 1 ATPase activity by troponin I and IC: relationship to the thin filament states of muscle. *Biochemistry* 39, 9345–9350 (2000).
34. Huxley, H. E. Structural changes in the actin- and myosin-containing filaments during contraction. *Cold Spring Harbor Symp. Quant. Biol.* 37, 361–376 (1972).
35. Haselgrove, J. C X-ray evidence for a conformational change in the actin-containing filaments of vertebrate striated muscle. *Cold Spring Harbor Symp. Quant. Biol.* 37, 341–352 (1972).
36. Parry, D. A. & Squire, J. M. Structural role of tropomyosin in muscle regulation: analysis of the x-ray diffraction patterns from relaxed and contracting muscles. *J. Mol. Biol.* 75, 33–55 (1973).
37. Hai, H., Sano, K., Maeda, K., Maéda, Y. & Miki, M. Ca^{2+}- and S1-induced conformational changes of reconstituted skeletal muscle thin filaments observed by fluorescence energy transfer spectroscopy: structural evidence for three states of thin filament. *J. Biochem. (Tokyo)* 131, 407–418 (2002).
38. Lehrer, S. S., Golitsina, N. L. & Geeves, M. A. Actin-tropomyosin activation of myosin subfragment 1 ATPase and thin filament cooperativity. The role of tropomyosin flexibility and end-to-end interactions. *Biochemistry* 36, 13449–13454 (1997).
39. Lorenz, M., Poole, K. J., Popp, D., Rosenbaum, G. & Holmes, K. C. An atomic model of the

unregulated thin filament obtained by X-ray fiber diffraction on oriented actin-tropomyosin gels. *J. Mol. Biol.* **246**, 108–119 (1995).
40. McKillop, D. F. & Geeves, M. A. Regulation of the interaction between actin and myosin subfragment 1: evidence for three states of the thin filament. *Biophys. J.* **65**, 693–701 (1993).
41. Fujita-Becker, S., Kluwe, L., Miegel, A., Maeda, K. & Maeda, Y. Reconstitution of rabbit skeletal muscle troponin from the recombinant subunits all expressed in and purified from *E. coli*. *J. Biochem. (Tokyo)* **114**, 438–444 (1993).
42. Otwinoski, Z. M. W. Processing of X-ray diffraction data collected in oscillation mode (eds Carter, C. W. & Sweet, R. M.) *Methods Enzymol* **276**, 307–326 (1997).
43. Terwilliger, T. C. & Berendzen, J. Automated MAD and MIR structure solution. *Acta. Crystallogr. D* **55**, 849–861 (1999).
44. de La Fortelle, E. & Bricogne, G. Maximum-likelihood heavy-atom parameter refinement for multiple isomorphous replacement and multiwavelength anomalous diffraction methods. (eds Carter, C. W. & Sweet, R. M.) *Methods Enzymol* **276**, 472–494 (1997).
45. Abrahams, J. P. & Leslie, A. G. W. Methods used in the structure determination of bovine mitochondrial F1 ATPase. *Acta Crystallogr. D* **52**, 30–42 (1996).
46. Roussel, A. & Cambillau, C. *TURBO-FRODO Manual* (AFMB-CNRS, Marseille, 1996).
47. Brunger, A. T. *et al.* Crystallography & NMR system: A new software suite for macromolecular structure determination. *Acta Crystallogr. D* **54**, 905–921 (1998).
48. CCP4 The CCP4 suite: programs for protein crystallography. *Acta. Crystallogr. D* **50**, 760–763 (1994).
49. Kraulis, P. J. MOLSCRIPT: a program to produce both detailed and schematic plots of protein structure. *Acta Crystallogr. D* **24**, 946–950 (1991).
50. Merritt, E. A. & Murphy, E. M. P. *Raster3D Version2.0—a program for photorealistic molecular graphics Acta Crystallogr. D* **50**, 869–873 (1994).

Supplementary Information accompanies the paper on **www.nature.com/nature.**

Acknowledgements We thank Y. Kawano, S. Adachi, S.-Y. Park, M. Kawamoto and K. Miura for technical help at the beam lines of SPring-8. We also thank S. Ebashi, I. Ohtsuki, F. Oosawa, K. Maruyama and T. Nitta for continuous support and encouragement throughout this work. This work was supported in part by Matsushita Electric Industrials, and by the Special Coordination Funds from the Ministry of Education, Culture, Sports, Science and Technology, Japan. We dedicate this paper to S. Ebashi.

Competing interests statement The authors declare that they have no competing financial interests.

Correspondence and requests for materials should be addressed to S.T. (stakeda@ri.ncvc.go.jp) or Y.M. (ymaeda@spring8.or.jp). Atomic coordinates and structure factors have been deposited in the Protein Data Bank under accession codes 1J1D for Tn46K and 1J1E for Tn52K.

Available online at www.sciencedirect.com
SCIENCE DIRECT®
Journal of Chromatography B, 798 (2003) 163–166
JOURNAL OF CHROMATOGRAPHY B
www.elsevier.com/locate/chromb

Short communication

Detection of 3-methoxy-4-hydroxyphenylglycol in rabbit skeletal muscle microdialysate

Noriyuki Tokunaga, Toji Yamazaki*, Tsuyoshi Akiyama, Hidezo Mori

Department of Cardiac Physiology, National Cardiovascular Center Research Institute, Fujishiro-dai 5-7-1, Suita, Osaka 565-8565, Japan

Received 24 June 2003; received in revised form 4 September 2003; accepted 8 September 2003

Abstract

A high-performance liquid chromatography with electrochemical detection (HPLC–ED) method is described for determination of 3-methoxy-4-hydroxyphenylglycol (MHPG) in microdialysate from the skeletal muscle interstitial space. Using a microdialysis technique, we sampled 30 μl dialysate from the skeletal muscle interstitial space and injected dialysate directly into HPLC–ED system. The control MHPG concentration of dialysate was 213 ± 18 pg/ml. The MHPG concentrations were reduced by entacapone (catechol-*O*-methyltransferase inhibitor, COMT), augmented by local infusion of dihydroxyphenylglycol. This system offers a new possibility for simple, rapid monitoring of MHPG as an index of COMT activity in skeletal muscle.

Keywords: 3-Methoxy-4-hydroxyphenylglycol

1. Introduction

3-Methoxy-4-hydroxyphenylglycol (MHPG) is a major metabolite of norepinephrine (NE) [1]. MHPG is produced by extra-neuronal *O*-methylation of 3,4-dihydroxyphenylglycol (DHPG) formed intraneuronally from NE or by the extra-neuronal combination of catechol-*O*-methyltransferase (COMT) and monoamine oxidase on NE. Microdialysis technique with high-performance liquid chromatography (HPLC) has been applied to monitor interstitial MHPG levels in the brain [2]. It is important for understanding the metabolic inactivation of NE to monitor MHPG production. Recently, it has been suggested that MHPG is a major extra-neuronal metabolite of NE in peripheral other organs including skeletal muscle [3]. Actually, the COMT activity is found in not only brain but also peripheral organs and tissues [4]. However, there has been no report monitoring peripheral MHPG levels by microdialysis technique with HPLC.

We previously reported that microdialysis technique with HPLC made it possible to directly measure the low levels of another important NE metabolite, DHPG in the cardiac myocardial interstitial space [5]. In the present study, we extend microdialysis technique with HPLC to the measurement of MHPG in skeletal muscle. We directly injected dialysate sample obtained from skeletal muscle to HPLC and analyzed dialysate MHPG concentration without internal standard or extraction procedure.

2. Experimental

2.1. Reagents

Distilled water and methanol were of HPLC grade from Wako Pure Chemical (Osaka, Japan). Standard solution of MHPG was obtained from Sigma (St. Lois, MO, USA) and 1-octane-sulfonic acid sodium salt was Nacalai Tesque (Kyoto, Japan). All other chemicals were of analytical grade and were used without any further pretreatment. A stock solution of MHPG was prepared separately at a concentration of 1 mg/l in 0.1 M perchloric acid. A working standard mixture containing (per liter) 100 ng of MHPG was made in Ringer's solution. Stock solutions were stable at 4 °C for 1 month.

* Corresponding author. Tel.: +81-6-6833-5012; fax: +81-6-6872-8092.
E-mail address: yamazaki@ri.ncvc.go.jp (T. Yamazaki).

1570-0232/$ – see front matter © 2003 Elsevier B.V. All rights reserved.
doi:10.1016/j.jchromb.2003.09.016

2.2. Dialysis probe and in vivo skeletal muscle dialysis

We designed a transverse dialysis probe. The dialysis fiber (13 mm length, 0.31 mm o.d., and 0.2 mm i.d.; PAN-1200, 50,000 molecular mass cut-off, Asahi chemical, Tokyo, Japan) was glued at both ends into a polyethylene tube (25 mm length, 0.5 mm o.d., and 0.2 mm i.d.) [6]. Eighteen male Japanese white rabbits weighing 2.5–2.8 kg each were anesthetized with pentobarbital sodium (30–35 mg/kg, i.v.). The level of anesthesia was maintained with a continuous intravenous infusion of pentobarbital sodium (1–2 mg/kg/h). The animals were intubated and ventilated with room air mixed with oxygen. Body temperature was maintained with a heating pad. All protocols were performed in accordance with the *National Cardiovascular Center Research Institute Animal Care Ethics Committee Guidelines*. Heart rate and arterial blood pressure were simultaneously monitored with a data recorder. After longitudinal skin incision of left groin, the dialysis probe was implanted in the left adductor muscle along with long axis. The dialysis probe was perfused with Ringer's solution at 10 μl/min using a microinjection pump (CMA 102, Carnegie Medicin, Stockholm, Sweden). We started the dialysate sampling followed by a stabilization period of 2 h. The concentrations of MHPG were measured at (1) the control state, (2) 60 min after intraperiotoneal injection of entacapone (COMT) inhibitor (10 mg/kg), and (3) 60 min after infusion of DHPG (25 ng/ml) through the dialysis probe. One sample period was 3 min (one dialysate sample volume = 30 μl). Each sample was collected in a 300 μl microtube containing 3 μl of 0.1N HCl to prevent amine oxidation.

2.3. Chromatographic and detection conditions

Using an autoinjector (CMA 200, Carnegie Medicin), 30 μl was injected into the liquid chromatograph. The HPLC system consisted of a pump with a pulse dumper (EP-300, Eicom, Kyoto, Japan), guard column (AC-ODS, 5 × 4 mm i.d., Eicom), analytic reversed-phase column (Eicompak CA-5ODS, 150 mm × 2.1 mm i.d., Eicom), an electrochemical detector equipped with a graphite electrode (ECD-300, Eicom), a chromato-integrator (D-2500, Hitachi, Tokyo, Japan) and a degasser (DG-300, Eicom). The mobile phase consisted of 1-octane-sulfonic acid sodium salt (200 mg/l in final concentration) in 0.1 M phosphate buffer (pH 6.0) and methanol (97:3, v/v). The flow-rate was 0.23 ml/min. The electrochemical detector was operated at +550 mV versus an Ag–AgCl reference electrode. The HPLC separation was performed at 25 °C. The concentration of MHPG was determined by measuring the peak height and corrected from the volume of the added HCl.

3. Results and discussion

When mobile phase was injected into HPLC, there was no peak corresponding in retention time to that of standard MHPG in chromatogram. A chromatogram of MHPG standard solution (60 pg/30 μl) is shown in Fig. 1. The calibration curve for MHPG peak height was linear in the concentration range of 0.9–60 (0.9, 3, 9, 30, and 60) pg per 30 μl injection. The r^2 value for MHPG was 0.9997. We could not prepare MHPG-free dialysate in the present study. Therefore, the accuracy and precision were studied with MHPG-free perfusate. Mean concentrations and coefficient variation (C.V.) with MHPG-free perfusate are presented in Table 1. In intra-day measurement, mean concentration ranged from 86 to 107% of theory and C.V. from 1 to 6% over 0.9 to 60 pg per injection of MHPG base concentration range. In inter-day measurement, mean concentration ranged form 93 to 105% of theory and C.V. from 3 to 10% over 0.9 to 60 pg per injection of MHPG base concentration.

When perfusate solution was injected into HPLC, there was no peak corresponding in retention time to that of standard MHPG in chromatogram. A peak corresponding in retention time to standard MHPG was estimated as MHPG peak. Fig. 1 shows typical chromatograms obtained from dialysate samples. MHPG peak height of dialysate was reduced by entacapone, and augmented by DHPG infusion. Furthermore, this DHPG-induced increment in MPHG peak height was canceled with the pretreatment of entacapone. The MHPG concentration of control dialysate was 213 ± 18 pg/ml ($n = 6$) (Fig. 2). Administration of entacapone significantly decreased the MHPG concentration of dialysate to 133 ± 16 pg/ml ($n = 5$). Local administration of DHPG increased the MHPG concentration of dialysate to 697 ± 265 pg/ml ($n = 5$). Thus, dialysate MHPG concentration reflects MHPG production and COMT activity at the skeletal muscle.

Using dialysate samples, we carried out preliminary validation study. We validated the accuracy of the method by spiking skeletal muscle dialysate with known amount of MHPG and calculate recovery. Dialysate samples were obtained from a rabbit, and we spiked the dialysate samples with known amount of MHPG (0.9, 3.0, and 6.0 pg). Peak corresponding in retention time to standard MHPG were linear and r^2 value was 0.982. The basal dialysate samples were spiked with MHPG in LOQ level (0.9 pg). Their MHPG levels with and without spiked MHPG (0.9 pg) were 5.6 ± 0.1, 6.5 ± 0.2 pg per injection ($n = 4$). Inter-day precision data were calculated from dialysate samples in two rabbits. Their C.V. values were 3.8 and 3.5%, respectively. Furthermore, the potential for electrochemical detector was re-set at 500 mV, dialysate peak corresponding in retention time to standard MHPG and standard MHPG peak were reduced in parallel. There are several peaks eluting between 4.5 and 5.5 min in dialysate samples. Changes in the concentration of anion-paring agent did not alter the retention

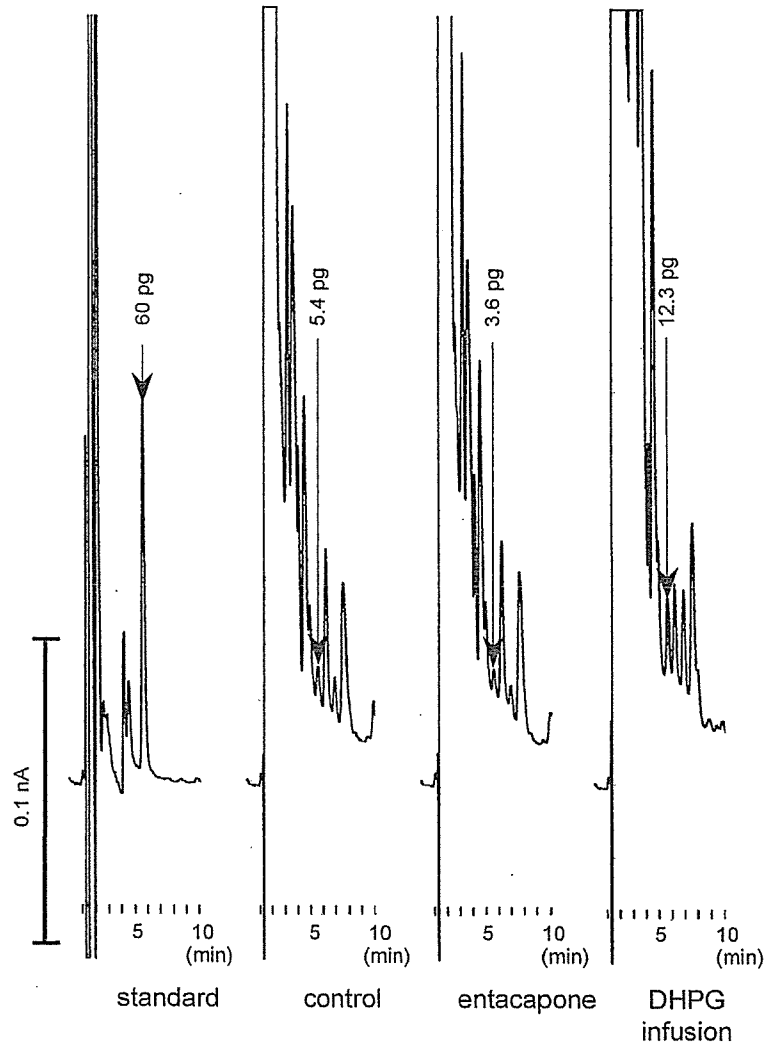

Fig. 1. Chromatograms of 3-methoxy-4-hydroxyphenylglycol (MHPG). The injection volume was 30 μl standard, 60 pg MHPG; control, skeletal muscle dialysate; entacapone, skeletal muscle dialysate after administration of entacapone; dihydroxyphenylglycol (DHPG) infusion, skeletal muscle dialysate after local infusion of DHPG through the dialysis probe.

time of MHPG but altered the retention times of interfering cross-peaks. Therefore, we carefully chose the concentration of anion-paring agent to avoid interfering cross peaks. Up to now, we have measured >200 dialysate samples and can say unequivocally that these peaks do not interfere the measurement of MHPG peak.

Thus, our method detects as little as 900 fg of MHPG per injection. Several studies on measurement of MHPG in plasma or urine were published [7–10]. Dialysate MHPG levels in the skeletal muscle range below their detection limit because their employed methods need complicated procedures, which attenuate their sensitivity. In this system,

Table 1
Intra- and inter-day accuracy and precision

Nominal/added concentration (pg per injection)	Intra-day			Inter-day		
	No. of values	Accuracy	Precision C.V. (%)	No. of values	Accuracy	Precision C.V. (%)
0.9	5	86	6	5	93	10
3	5	99	2	5	105	6
6	5	107	2	5	102	4
30	5	99	1	5	100	3
60	5	103	2	5	96	5

Accuracy: mean found concentration (% of nominal). C.V.: coefficient variation (CV) of the mean concentration. Standard MHPG was dissolved in Ringer's solution.

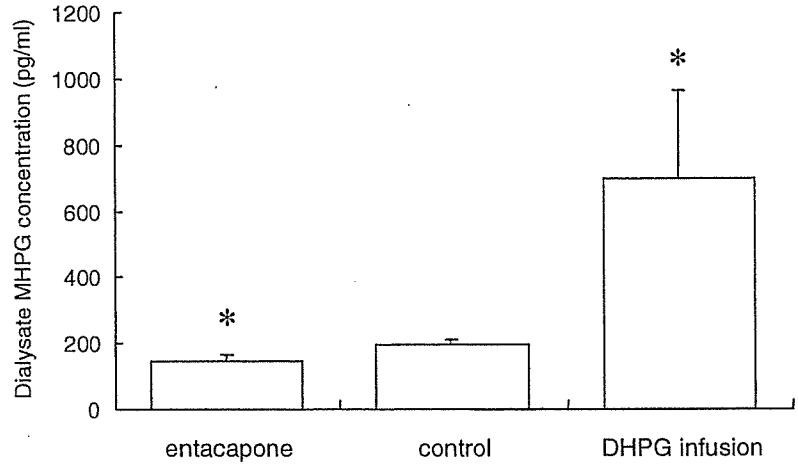

Fig. 2. Effects of entacapone (COMT inhibitor) or dihydroxyphenylglycol (DHPG) on dialysate 3-methoxy-4-hydroxyphenylglycol (MHPG) concentrations. Intraperitoneal administration of entacapone decreased dialysate MHPG concentrations and DHPG infusion through dialysis probe increased dialysate MHPG concentrations. Values are means ± S.E. $^*P < 0.05$ vs. value of control.

quantification limit of MHPG was comparable to those of NE and DHPG. For each measurement of NE, DHPG and MHPG, we employed the same HPLC–ED apparatus but separate own system. Chromatographic condition in mobile phase component and flow rate, were chosen for highly sensitive measurement of MHPG. Further, sample from plasma or urine need extraction procedure for eliminating many possible interferences [7]. Extraction procedure restricts highly sensitive measurement. When dialysate from the skeletal muscle was injected to HPLC–ED, the low concentration of MHPG was detectable and reproducible without extraction or internal standard.

To our knowledge, this is the first report on the in vivo measurement of MHPG by direct injection of dialysate obtained from skeletal muscle to HPLC–ED system without internal standard or complex extraction procedure. Early study suggested that majority of MHPG in plasma was derived from skeletal muscle in human study [3]. Therefore, measurement of MHPG in skeletal muscle may be particularly appropriate for providing information about the mechanism of peripheral MHPG production. In this study, administration of COMT inhibitor significantly decreased the MHPG concentrations of dialysate and local administration of DHPG significantly increased the MHPG concentrations. Therefore, we consider that the concentration of MHPG in the skeletal muscle dialysate might correspond to the COMT activity in the skeletal muscle. Taken together with measurement of NE and DHPG, these analyses yield new approach to norepinephrine kinetics in the skeletal muscle. This system offers a simple, rapid monitoring of skeletal muscle MHPG concentrations as an index of in vivo COMT activity.

Acknowledgements

This work was supported by Grants-in-Aid for Scientific Research (13470154, 13877114).

References

[1] G. Eisenhofer, W. Pecorella, K. Pacak, D. Hooper, I.J. Kopin, D.S. Goldstein, J. Auton. Nerv. Syst. 50 (1994) 93.
[2] J.M. Duine, F. Floch, C. Cann-Moisan, P. Mialon, J. Caroff, J. Chromatogr. B 716 (1998) 350.
[3] G.W. Lambert, D.M. Kaye, M. Vaz, H.S. Cox, A.G. Turner, G.L. Jennings, M.D. Esler, J. Auton. Nerv. Syst. 55 (1995) 169.
[4] P. Männistö, S. Kaakkola, Pharmacol. Rev. 51 (1999) 593.
[5] Y. Takauchi, H. Kitagawa, T. Kawada, T. Akiyama, T. Yamazaki, J. Chromatogr. B 693 (1997) 218.
[6] T. Akiyama, T. Yamazaki, I. Ninomiya, Am. J. Physiol. 30 (1991) 1643.
[7] M. Hariharan, T. VanNoord, O.G. Cameron, G.C. Curtis, D.G. Ostrow, Clin. Chem. 35 (1989) 202.
[8] J. Semba, A. Watanabe, R. Takahashi, Clin. Chim. Acta 152 (1985) 185.
[9] E. Hollenbach, C. Schulz, H. Lehnert, Life Sci. 63 (1998) 737.
[10] N.S. Sharpless, U. Halbreich, H. Feldfogel, J. Chromatogr. 377 (1986) 101.

Available online at www.sciencedirect.com
SCIENCE DIRECT®
Neurochemistry International 43 (2003) 573–580
NEUROCHEMISTRY International
www.elsevier.com/locate/neuint

In vivo monitoring of norepinephrine and its metabolites in skeletal muscle

Noriyuki Tokunaga [a], Toji Yamazaki [a,*], Tsuyoshi Akiyama [a], Shunji Sano [b], Hidezo Mori [a]

[a] *Department of Cardiac Physiology, National Cardiovascular Center Research Institute, 5-7-1 Fujishiro-dai, Suita, Osaka 565-8565, Japan*
[b] *Department of Cardiovascular Surgery, Okayama University Medical School, Okayama 700-8558, Japan*

Received 2 October 2002; accepted 10 January 2003

Abstract

Although skeletal muscle sympathetic nerve activity plays an important role in the regulation of vascular tone and glucose metabolism, relatively little is known about regional norepinephrine (NE) kinetics in the skeletal muscle. With use of the dialysis technique, we implanted dialysis probes in the adductor muscle of anesthetized rabbits and examined whether dialysate NE and its metabolites were influenced by local administration of pharmacological agents through the dialysis probes. Dialysate dihydroxyphenylglycol (DHPG) and 3-methoxy-4-hydroxyphenylglycol (MHPG) were measured as two major metabolites of NE. The skeletal muscle dialysate NE, DHPG and MHPG were 11.7 ± 1.2, 38.1 ± 3.2, and 266.1 ± 28.7 pg/ml, respectively. Basal dialysate NE levels were suppressed by tetrodotoxin (Na^+ channel blocker, 10 μM) (5.1 ± 0.6 pg/ml), and augmented by desipramine (NE uptake blocker, 100 μM) (25.8 ± 3.2 pg/ml). Basal dialysate DHPG levels were suppressed by pargyline (monoamine oxidase blocker, 1 mM) (24.3 ± 4.6 pg/ml) and augmented by reserpine (vesicle NE transport blocker, 10 μM) (75.8 ± 2.7 pg/ml). Basal dialysate MHPG levels were not affected by pargyline, reserpine, or desipramine. Addition of tyramine (sympathomimetic amine, 600 μM), KCl (100 mM), and ouabain (Na^+–K^+ ATPase blocker, 100 μM) caused brisk increases in dialysate NE levels (200.9 ± 14.2, 90.6 ± 25.7, 285.3 ± 46.8 pg/ml, respectively). Furthermore, increases in basal dialysate NE levels were correlated with locally administered desipramine (10, 100 μM). Thus, dialysate NE and its metabolite were affected by local administration of pharmacological agents that modified sympathetic nerve endings function in the skeletal muscle. Skeletal muscle microdialysis with local administration of a pharmacological agent provides information about NE release, uptake, vesicle uptake and degradation at skeletal muscle sympathetic nerve endings.

Keywords: Dihydroxyphenylglycol; 3-Methoxy-4-hydroxyphenylglycol; Microdialysis; Rabbit; Skeletal muscle

1. Introduction

Muscle sympathetic nerve activity exerts an important action on the regulation of vascular tone (Lundvall and Edfeldt, 1994) and glucose metabolism (Fagius and Berne, 1994; Spraul et al., 1994) in the skeletal muscle. Clinical and experimental studies suggest that alterations of sympathetic nerve function at the skeletal muscle are involved in the pathogenesis of various diseases (Cabassi et al., 2001; Grassi et al., 1995). Further, organ-specific norepinephrine (NE) spillover demonstrated that as much as 20% of the norepinephrine entering plasma derives from the skeletal muscle (Esler et al., 1984). Thus, norepinephrine kinetics in the skeletal muscle plays an important role in various physiological and pathophysiological conditions. However, owing to methodological problems, relatively little is known about NE kinetics in the skeletal muscle.

To elucidate NE kinetics at the sympathetic nerve endings, NE release, uptake, vesicle transport, vesicle storing capacity and metabolism should be assessed. Until now, available methodology for examination of nerve endings function has been limited to assessment of radiolabelled-NE kinetics. In practice, this sophisticated technique has provided a powerful method for the analysis of heart (Thompson et al., 1998), kidney (Wallin et al., 1996) and liver (Aneman et al., 1996; Mundinger et al., 1997). However, dispersed organ systems, such as skeletal muscle and skin are not suitable for NE spillover. On the other hand, muscle sympathetic nerve activity was recorded by microneurography (Anderson et al., 1989; Ferguson et al., 1990). This technique provides information only about NE releasing function, while NE uptake, NE metabolism and other functions remain unclear.

Recently microdialysis technique in combination with a high-performance liquid chromatographic method with

* Corresponding author. Tel.: +81-6-6833-5012; fax: +81-6-6872-8092.
E-mail address: yamazaki@ri.ncvc.go.jp (T. Yamazaki).

0197-0186/03/$ – see front matter © 2003 Elsevier Science Ltd. All rights reserved.
doi:10.1016/S0197-0186(03)00064-0

electrochemical detection (HPLC-ED) has offered a unique and powerful method for analysis of NE kinetics in cardiac sympathetic nerve endings (Takauchi et al., 1997; Yamazaki et al., 1995, 1997). This method is suitable for probe-implantable organs, such as heart, kidney (Zou and Cowley, 1997), brain (Kiss et al., 1995) and adipose tissue (Arner et al., 1988). Modification of the analytical conditions for the HPLC-ED system may allow extension of this method to skeletal muscle as well. Measurement of NE and its metabolites in the skeletal muscle could be particularly appropriate to gain information about skeletal muscle-specific sympathetic nerve endings function (Bruce et al., 2002; Gronlund et al., 1991). In the present study, to examine basal NE kinetics at the skeletal muscle sympathetic nerve endings, we performed skeletal muscle dialysis in combination with local administration of various neuropharmacological drugs.

2. Methods

2.1. Animal preparation

Male Japanese white rabbits weighing 2.5–3 kg each were anesthetized with pentobarbital sodium (30–35 mg/kg, i.v.). The level of anesthesia was maintained with a continuous intravenous infusion of pentobarbital sodium (1–2 mg/kg h). The animals were intubated and ventilated with room air mixed with oxygen. Body temperature was maintained with a heated pad and lamp. All protocols were performed in accordance with the American Physiological Society guidelines for the use of animals. An electrocardiogram, heart rate, and arterial blood pressure were simultaneously monitored with a data recorder. After a longitudinal skin incision of left groin was made, the dialysis probes were implanted in the left adductor muscle with a fine guiding needle (Fig. 1). To compare dialysate NE and its metabolites between skeletal and cardiac muscle, in some of the experiments, we implanted a dialysis probe in the left ventricle free wall in the heart.

2.2. Dialysis technique

With the dialysis technique, dialysate NE and its metabolite concentrations were measured as an index of skeletal muscle interstitial levels. For skeletal muscle dialysis, we designed a transverse dialysis probe. The dialysis fiber (13 mm length, 0.31 mm o.d. and 0.2 mm i.d.; PAN-1200, 50,000 molecular mass cut-off, Asahi Chemical, Tokyo, Japan) was glued at both ends into a polyethylene tube (25 cm length, 0.5 mm o.d. and 0.2 mm i.d.) (Akiyama et al., 1991). The dialysis probe was perfused with Ringer solution at a speed of 10 μl/min using a microinjection pump (CMA 102, Carnergie Medicin, Stockholm, Sweden). One sampling period was 10 min (one dialysate sample volume: 100 μl). In the preliminary experiment, we examined the time course of dialysate NE levels at 30–60 min interval over a period of 240 min ($n = 3$). Dialysate NE levels were 21.1 ± 8.0 pg/ml at 30 min after probe implantation, then decreased to 9.0 ± 0.3 pg/ml at 90 min after implantation. Thereafter, it reached an almost steady level at 120–240 min after probe implantation. Therefore, dialysate sampling was started 120 min after probe implantation in the experimental protocol. Each sample was collected in a 300 μl microtube containing 10 μl of 0.1N HCl, to prevent amine oxidation.

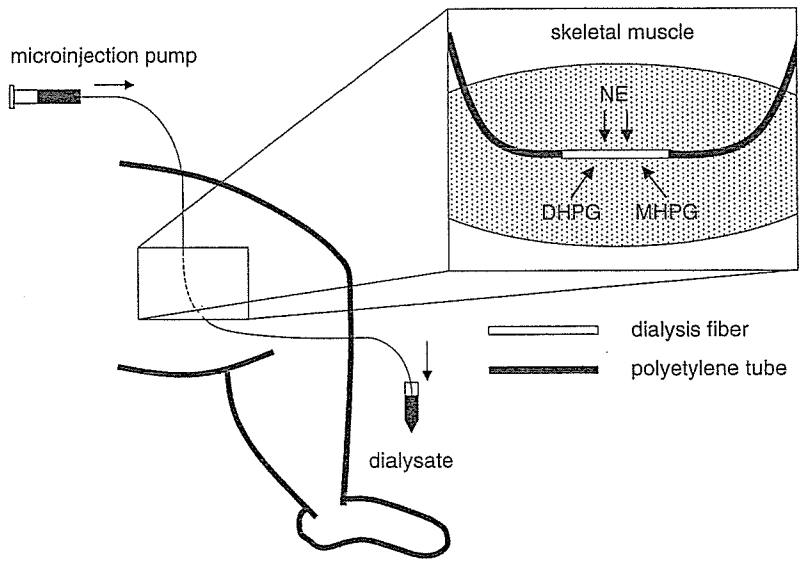

Fig. 1. Dialysis technique in skeletal muscle. Dialysis probe was implanted in adductor muscle with a fine guiding needle and perfused with Ringer solution containing neuropharmacological agents using a microinjection pump. NE: norepinephrine; DHPG: dihydroxyphenylglycol; MHPG: 3-methoxy-4-hydroxyphenylglycol.

2.3. Experimental protocols

In the present study, to examine basal NE kinetics at the skeletal muscle sympathetic nerve endings, we performed skeletal muscle dialysis in combination with local administration of various neuropharmacological drugs. We referred to the previous experiments on the measurement of cardiac dialysate to determine the concentrations of pharmacological agents and sampling time (Akiyama et al., 1991; Yamazaki et al., 1997).

2.3.1. Protocol 1: source of dialysate NE in skeletal muscle

Interstitial NE derived mainly from circulating NE and/or regional sympathetic nerve endings. It is unclear to what extent regional sympathetic nerve endings contribute to change in dialysate NE. To elucidate the source of dialysate NE in the skeletal muscle, we modulated local NE releasing and up-taking function by local administration of a blocking agent. Tetrodotoxin (TTX, NE release blocker, 10 μM) or desipramine (NE uptake blocker: 10, 100 μM) was locally administered through the dialysis probe. Dialysate NE measurement was performed before, 30, and 60 min after the administration.

2.3.2. Protocol 2: influence of neuronal NE release and storage of NE on dialysate NE levels

To examine NE releasing function in skeletal muscle sympathetic nerve endings, we locally administered high K^+ (KCl 100 mM) and ouabain (Na^+–K^+ ATPase blocker, 100 μM) through the dialysis probes, and obtained the dialysate NE responses. Furthermore, to examine storage capacity of NE in skeletal muscle sympathetic nerve endings, we locally administered tyramine (NE releasing sympathomimetic amine, 600 μM) through the dialysis probe (Takauchi et al., 2000). Dialysate NE measurement was performed before, 0–10, and 10–20 min after the administration of KCl or tyramine. In the case of ouabain, to compare the response with the previous studies on cardiac dialysis, one sampling period was set at 15 min and ouabain was locally administered for 60 min (Yamazaki et al., 2001b).

2.3.3. Protocol 3: influence of axoplasmic NE disposition on dialysate dihydroxyphenylglycol (DHPG) levels

The released NE is mainly re-uptaken and mobilized into the stored NE vesicle. Furthermore, axoplasmic NE is partially metabolized with monoamine oxidase (MAO) (Youdim et al., 1988). DHPG is a major metabolite of NE with MAO and served as an index of axoplasmic NE levels (Kopin, 1985). To examine whether dialysate DHPG level reflects axoplasmic NE disposition, we locally administered these neuronal pathway inhibitors and measured dialysate DHPG levels. Pargyline (MAO inhibitor, 1 mM), reserpine (vesicle NE transport inhibitor, 10 μM), or desipramine (100 μM) was separately administered, and dialysate DHPG responses were measured.

2.3.4. Protocol 4: influence of axoplasmic NE disposition on dialysate 3-methoxy-4-hydroxyphenylglycol (MHPG) levels

MHPG is produced by extraneuronal *O*-methylation of DHPG and by the extraneuronal combination of catechol *O*-methyltransferase (COMT) and MAO on NE (Kopin, 1985). We examined the effects of pargyline (1 mM), reserpine (10 μM) and desipramine (100 μM) on dialysate MHPG levels.

2.3.5. Protocol 5: comparison of dialysate NE and its metabolites between cardiac and skeletal muscle

In previous papers, we performed cardiac microdialysis for myocardial interstitial NE and DHPG measurements (Akiyama et al., 1991; Yamazaki et al., 1997). Although the details of measurements have already been reported, whether dialysate NE and its metabolites in cardiac muscle are comparable to those in skeletal muscle remains unclear. We measured dialysate NE and its metabolites in myocardial interstitium in separate rabbits. To compare the results in cardiac and skeletal muscle, the levels of NE and its metabolites in cardiac muscle were corrected by the difference of the in vitro NE recovery rates, and the data were expressed as the level of NE and its metabolites in dialysate.

2.4. Analytical procedure

Half of the dialysate sample was used for the NE measurement, and the remaining sample was split for the DHPG and MHPG measurements. Dialysate NE concentrations were measured by HPLC-ED (Eicom, Japan) after removing interfering compounds by an alumina procedure (Anton and Sayer, 1962). The dialysate DHPG and MHPG were measured directly by two other HPLC-ED. Details of HPLC-ED for NE and DHPG measurements have been described elsewhere (Takauchi et al., 1997; Yamazaki et al., 1995). The dialysate MHPG was measured directly by another HPLC-ED. Separation was performed using an analytical reverse-phase column with a flow of 0.2 ml/min. The amperometric detector was operated at 0.55 V versus an Ag/AgCl reference electrode. The mobile phase consisted of l-octane-sulfonic sodium salt (200 mg/l final concentration) in 0.1 M phosphate buffer (pH 6.0) and methanol (97:3, v/v). The limit of quantification for MHPG was 900 fg in a 30 μl injection.

2.5. Materials

The following drugs were used: TTX (Wako Pure Chemical Co., Osaka, Japan), desipramine (Sigma), KCl (Wako Pure Chemical), ouabain (Sigma), tyramine (Sigma), pargyline (Sigma), reserpine (Daiichi Pharmaceutical Co., Tokyo, Japan).

At the end of each experiment, the rabbits were killed with an overdose of pentobarbital sodium and the implant sites were checked to confirm that the dialysis probes had

been implanted within the left adductor muscle. Statistical analysis of the data was performed by analysis of variance (ANOVA) followed by Scheffé's F, Dunnett's post-hoc procedure. Paired t-test was applied to analyze the dialysate DHPG levels before and after administration of pharmacological drugs. Statistical significance was defined as $P < 0.05$. Values are presented as mean ± S.E.

3. Results

Hemodynamic variables of arterial pressure and heart rate were unaltered during local administration of the pharmacological agents. Further, no arrhythmia occurred during the experimental study.

3.1. Protocol 1: source of dialysate NE in skeletal muscle

Fig. 2 shows dialysate NE levels before and after local administration of TTX (10 μM) or desipramine (100 μM). Local administration of TTX significantly decreased the dialysate NE levels from 15.4 ± 2.4 to 5.1 ± 0.6 pg/ml at 30 min of administration. This decrease in dialysate NE was preserved at 60 min of administration. Local administration of desipramine significantly increased the dialysate NE levels from 11.1 ± 1.4 to 25.8 ± 3.2 pg/ml at 30 min of administration. This increase was also preserved during the administration. Furthermore, the increase in dialysate NE (18.7 ± 2.9 pg/ml) was observed at 10 μM of desipramine. Increases in dialysate NE levels were correlated with locally administered desipramine (10, 100 μM).

3.2. Protocol 2: influence of neuronal NE release and storage of NE on dialysate NE levels

Fig. 3 shows the time course of local administration of tyramine (600 μM) or KCl (100 mM). Local administration of tyramine significantly increased the dialysate NE levels from 23.9 ± 2.7 to 200.9 ± 14.2 pg/ml. Local administration of KCl significantly increased the dialysate NE levels from 11.7 ± 2.8 pg/ml at control to 84.7 ± 20.8 pg/ml at 10 min, 90.6 ± 25.7 pg/ml at 20 min. Fig. 4 shows the time course of the dialysate NE levels during local administration of ouabain (100 μM). Local administration of ouabain significantly increased the dialysate NE levels from 17.8 ± 2.0 pg/ml at control to 57.2 ± 21.2 pg/ml at 15 min, 206.9 ± 48.3 pg/ml at 30 min, and 285.3 ± 46.8 pg/ml at 45 min. Subsequently, a slow decline occurred but high dialysate levels were maintained during locally applied ouabain.

3.3. Protocol 3: influence of axoplasmic NE disposition on dialysate DHPG levels

Fig. 5 shows dialysate DHPG levels in various conditions. Local administration of pargyline (1 mM) significantly decreased dialysate DHPG levels from 39.4 ± 6.6 pg/ml at control to 24.3 ± 4.6 pg/ml. Local administration of reserpine (10 μM) significantly increased dialysate DHPG levels from 35.0 ± 4.7 to 75.8 ± 2.7 pg/ml. Local administration of desipramine (100 μM) did not affect dialysate DHPG levels.

3.4. Protocol 4: influence of axoplasmic NE disposition on dialysate MHPG levels

Dialysate MHPG levels averaged 212.4 ± 6.5 pg/ml at control. Local administration of pargyline (1 mM), reserpine (10 μM) and desipramine (100 μM) did not affect dialysate MHPG levels (pargyline: 170.7 ± 8.9, reserpine: 247.4 ± 20.5, desipramine 197.5 ± 15.5 pg/ml).

3.5. Protocol 5: comparison of dialysate NE and its metabolites between cardiac and skeletal muscle

Basal cardiac dialysate NE, DHPG, and MHPG levels were 57.3 ± 13.7, 353.1 ± 53.4, and 447.3 ± 64.3 pg/ml, respectively (Table 1). Basal skeletal muscle dialysate NE,

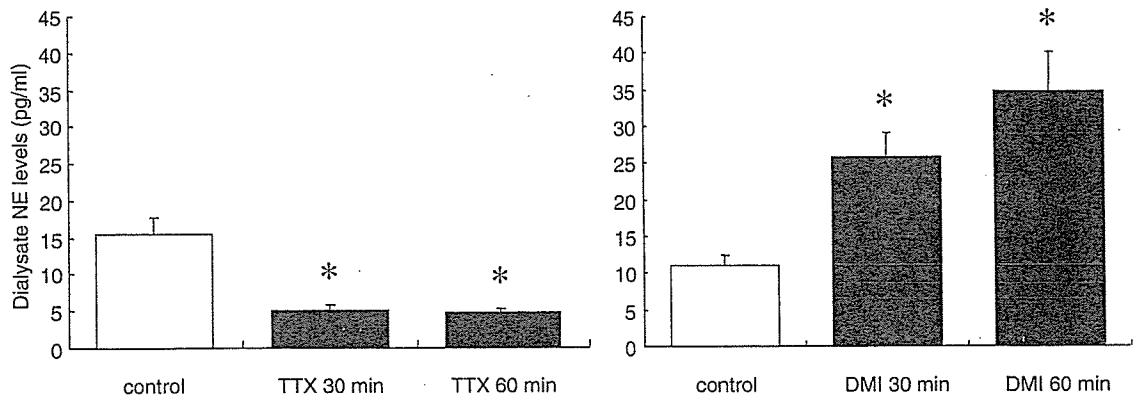

Fig. 2. Local administration of TTX (10 μM) markedly decreased the dialysate NE levels ($n = 7$). In contrast, DMI (100 μM) significantly increased the dialysate NE levels. NE: norepinephrine; TTX: tetrodotoxin; DMI: desipramine. $^*P < 0.05$ vs. control.

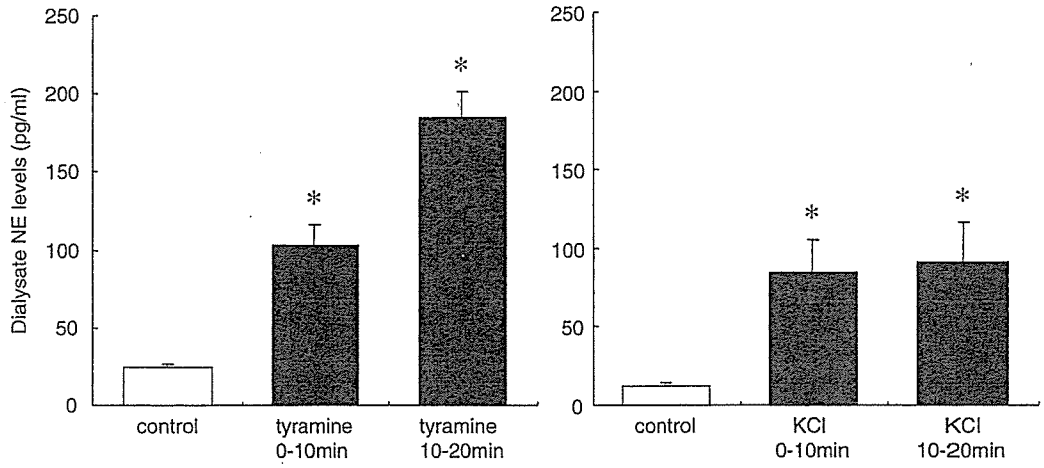

Fig. 3. Local administration of tyramine (600 μM ($n = 6$)) and KCl (100 mM ($n = 5$)) markedly increased the dialysate NE levels. NE: norepinephrine. $^*P < 0.05$ vs. control.

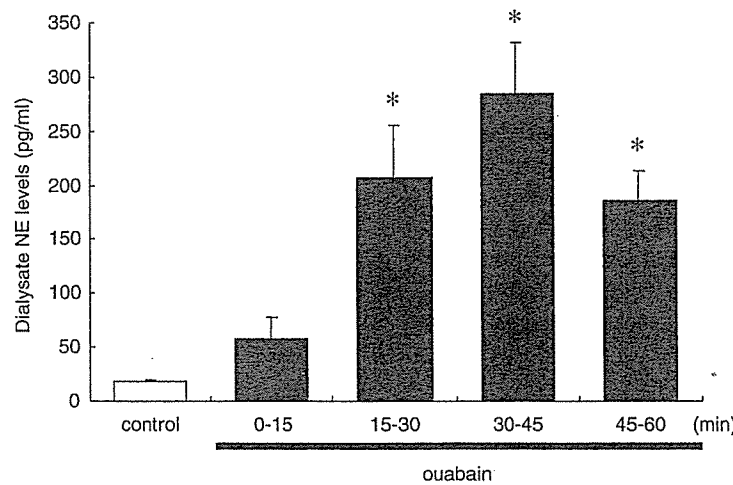

Fig. 4. Time course of the dialysate NE levels during ouabain (100 μM) administration ($n = 6$). NE: norepinephrine. $^*P < 0.05$ vs. control.

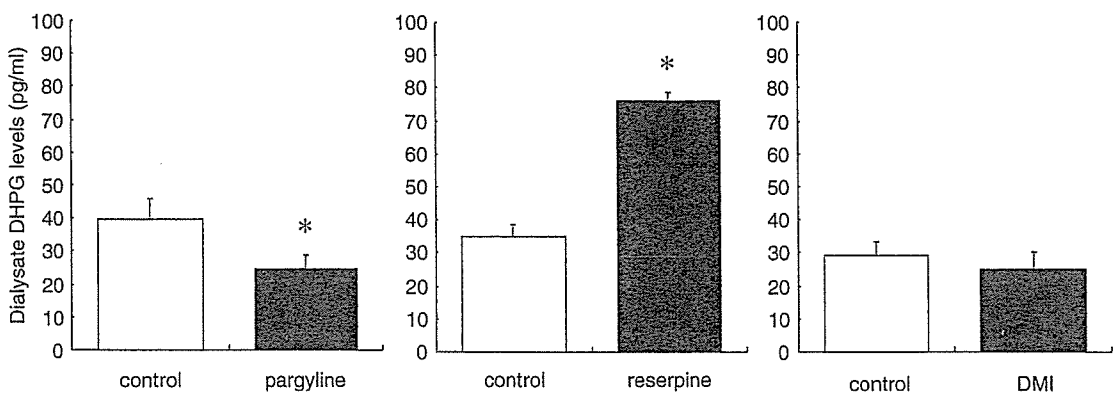

Fig. 5. Local administration of pargyline (1 mM) decreased dialysate DHPG levels ($n = 7$). Reserpine (10 μM) increased dialysate DHPG levels ($n = 5$). DHPG: dihydroxyphenylglycol; DMI: desipramine. $^*P < 0.05$ vs. control.

Table 1
Comparison of dialysate NE and its metabolites between cardiac and skeletal muscle

	Cardiac muscle	Skeletal muscle
NE (pg/ml)	57.3 ± 13.7	11.7 ± 1.2
DHPG (pg/ml)	353.1 ± 53.4	38.1 ± 3.2
MHPG (pg/ml)	447.3 ± 64.3	266.1 ± 28.7

NE: norepinephrine; DHPG: dihydroxyphenylglycol; MHPG: 3-methoxy-4-hydroxyphenylglycol.

DHPG, and MHPG levels averaged 11.7 ± 1.2, 38.1 ± 3.2, and 266.1 ± 28.7 pg/ml, respectively.

4. Discussion

At the skeletal muscle, the small amount of dialysate NE and its metabolites could be determined by the microdialysis coupling with electrochemical detection. The levels of interstitial NE and its metabolites might be affected by circulating NE and surrounding sympathetic tissue. Local administration of TTX markedly decreased dialysate NE. Our data suggest that the reduction of dialysate NE was derived from surrounding sympathetic nerve and remaining amount of NE was derived from circulating NE. Furthermore, desipramine increased dialysate NE. These results suggest that basal NE levels in dialysate were regulated by depolarization-induced exocytotic NE release and NE uptake. Therefore, function of surrounding sympathetic nerve endings was responsible for the basal dialysate NE level. This result is consistent with an early study in which the plasma NE level in vein draining skeletal muscle was noted to be higher than the arterial plasma level, indicating regional production of NE from sympathetic nerve endings (Esler et al., 1987). The dialysate DHPG levels were also altered by local administration of pargyline and reserpine which affected intraneuronal compartments. Both dialysate NE and its metabolite were derived mainly from surrounding sympathetic nerve endings. Thus, skeletal muscle NE and its metabolites reflect information about regional NE kinetics.

Data on NE spillover suggested that as much as 20–30% of the NE entering the circulation derived from skeletal muscle sympathetic nerves (Esler et al., 1984). Therefore, it is important to determine the function of NE release from skeletal muscle sympathetic nerves. Assessment of NE release from sympathetic nerve endings was performed with local administration of high K^+ and ouabain through the dialysis probe. Both high K^+ and ouabain induced increases in dialysate NE levels. On the other hand, cardiac NE spillover accounts for 2–3% of total body NE release to plasma (Esler et al., 1984), and high K^+ and ouabain-induced NE responses were five-fold higher than those of skeletal muscle (Yamazaki et al., 1998, 1999). In contrast to a dense innervated cardiac sympathetic nerve, the skeletal muscle has a thin sympathetic innervation, but organ mass or blood flow contributes to a large amount of NE spillover from the skeletal muscle. Thus, little increments in NE release at the skeletal muscle sympathetic nerve may affect circulating plasma NE levels.

In experimental or clinical conditions, sympathetic nerve innervation was determined pharmacologically by responsiveness to tyramine (Shannon et al., 2000; Takauchi et al., 2000). In in situ innervated skeletal muscle, local administration of tyramine caused a brisk increase in dialysate NE levels. High K^+ and tyramine induced increments in dialysate NE. These drugs act with different NE releasing mechanisms (Nicholls, 1994). Local administration of tyramine acted by releasing NE from stored vesicle with membrane and vesicle NE transporters (Langeloh et al., 1987; Trendelenburg et al., 1987). The level of dialysate NE evoked by tyramine seems to reflect the total NE content at the nerve endings. Therefore, the dialysate response could examine whether sympathetic nerve endings preserve vesicle NE content, membrane and vesicle NE transporters.

Data on experimental hypertension in rats demonstrated that NE uptake is impaired in skeletal muscle (Cabassi et al., 2001). Reduced NE uptake may be responsible for pathogenesis of hypertension. Microdialysis with local administration of pharmacological agents is particularly appropriate to identify impairment of regional NE uptake function (Yamazaki et al., 1997). Neuronal NE uptake function was assessed by local administration of desipramine. Desipramine induced an increment in dialysate NE but did not affect dialysate DHPG levels. Desipramine induced a two-fold increase in dialysate NE. Early studies indicate that this ratio is independent of NE release, but instead dependent on NE uptake function (Yamazaki and Akiyama, 1996; Yamazaki et al., 1997). Therefore, a comparison of the dialysate NE level between the presence and absence of desipramine reveals that neuronal NE uptake, to a variable extent, is involved in dialysate NE changes.

DHPG is a deaminated metabolite of NE (Kopin, 1985). Previous studies in cardiac microdialysis reported that, in the presence of an intact MAO system, DHPG serves as an index of the cytosolic (axoplasmic) NE level (Yamazaki et al., 1997, 2001a). Basal DHPG levels were altered by local administration of reserpine, but not by desipramine. These data suggested that basal dialysate DHPG level corresponds to vesicle NE mobilization rather than membrane NE uptake. Therefore these data support the conclusion that the production of DHPG is mainly due to intraneuronal MAO at surrounding skeletal muscle sympathetic nerve endings and that measurement of dialysate DHPG provides information about organ-specific vesicular uptake function rather than membrane NE uptake.

Basal dialysate MHPG level was higher than basal DHPG level. MHPG is also a major metabolite of NE. MHPG is produced by extraneuronal *O*-methylation of DHPG formed intraneuronally from NE or by the extraneuronal combination of COMT and MAO on NE (Kopin, 1985). Higher MHPG levels may suggest activity of extraneuronal NE degradation in physiological conditions. In fact, Lambert et al. described that the majority of MHPG in plasma is

derived from skeletal muscle (Lambert et al., 1995). Our data suggested that alteration of intraneuronal NE metabolism did not affect dialysate MHPG levels. Acute reflex stimulation of sympathetic nerve activity was not associated with parallel changes in regional MHPG production (Lambert et al., 1995). Further studies concerning the role of MHPG on skeletal muscle NE kinetics are warranted.

4.1. Methodological consideration

Several limitations and problems cast doubt on the validity of microdialysis technique as an index of regional sympathetic nerve function. The first limitation is related to the fact that we investigated the skeletal muscle NE and its metabolites in rabbits anesthetized with pentobarbital sodium. The anesthesia affects both the afferent and efferent sympathetic nerve tracts, and so may modify the NE response (Zimpfer et al., 1982). We agree with the influence of anesthesia on the autonomic control. Our final goal of these experiments is to investigate the skeletal muscle NE kinetics in conscious animals and clinical fields. Further studies concerning non-anesthetized animals and humans are warranted.

The second problem is related to the origin and physiological implication of sympathetic nerve endings in skeletal muscle. At the skeletal muscle, sympathetic nerve endings are histochemically located in blood vessels, muscle spindle, and skeletal muscle fibers (Barker and Saito, 1981). However, it is uncertain whether the obtained NE is derived mainly from specific sites and in what proportion. Furthermore, the sympathetic system can influence skeletal muscle contraction (Grassi and Passatore, 1988, 1990), blood flow (Lundvall and Edfeldt, 1994; Thompson and Mohrman, 1983), and glucose metabolism (Fagius and Berne, 1994; Spraul et al., 1994). The functional implications of NE release are an important focus for future studies.

Dialysis technique was used to determine interstitial NE and its metabolites in the heart and skeletal muscle. Basal NE level in the heart was five-fold higher than that of the skeletal muscle. Cardiac DHPG level was nine-fold higher than that of skeletal muscle. MHPG level in the heart was slightly higher than that of skeletal muscle. These studies show that intraneuronal NE turnover was more active in the heart, but in the skeletal muscle intraneronal NE turnover was less active and extraneuornal NE degradation was more active. Eisenhofer suggested that most released NE was captured by the NE uptake system, whereas extracted NE through the circulating NE might be captured by the extraneuronal NE uptake system (Eisenhofer, 2001). Dispersed organ systems, such as skeletal muscle, have a thin and diffuse sympathetic innervation, but being a large organ mass, the skeletal muscle NE and its metabolites cannot be ignored.

Acknowledgements

This work was supported by Grants-in-Aid for scientific research (13470154, 13877114) from the Ministry of Education, Culture, Sports, Science and Technology; New Energy and Industrial Technology Development Organization; the Research Grants for Cardiovascular Disease (H13C-1) from the Ministry of Health, Labor and Welfare; the Promotion Fundamental Studies in Health Science of the Organization for Pharmaceutical Safety and Research of Japan.

References

Akiyama, T., Yamazaki, T., Ninomiya, I., 1991. In vivo monitoring of myocardial interstitial norepinephrine by dialysis technique. Am. J. Physiol. 261, H1643–H1647.

Anderson, E.A., Sinkey, C.A., Lawton, W.J., Mark, A.L., 1989. Elevated sympathetic nerve activity in borderline hypertensive humans. Evidence from direct intraneural recordings. Hypertension 14, 177–183.

Aneman, A., Eisenhofer, G., Olbe, L., Dalenback, J., Nitescu, P., Fandriks, L., Friberg, P., 1996. Sympathetic discharge to mesenteric organs and the liver. Evidence for substantial mesenteric organ norepinephrine spillover. J. Clin. Invest. 97, 1640–1646.

Anton, A.H., Sayer, D.F., 1962. A study of the factors affecting the aluminum oxide-trihydroxyindole procedure for the analysis of catecholamine. J. Pharmacol. Exp. Ther. 138, 360–375.

Arner, P., Bolinder, J., Eliasson, A., 1988. Microdialysis of adipose tissue and blood for in vivo lipolysis studies. Am. J. Physiol. 255, E737–E742.

Barker, D., Saito, M., 1981. Autonomic innervation of receptors and muscle fibres in cat skeletal muscle. Proc. R. Soc. Lond. B: Biol. Sci. 212, 317–332.

Bruce, S., Tack, C., Patel, J., Pacak, K., Goldstein, D.S., 2002. Local sympathetic function in human skeletal muscle and adipose tissue assessed by microdialysis. Clin. Auton. Res. 12, 13–19.

Cabassi, A., Vinci, S., Quartieri, F., Moschini, L., Borghetti, A., 2001. Norepinephrine reuptake is impaired in skeletal muscle of hypertensive rats in vivo. Hypertension 37, 698–702.

Eisenhofer, G., 2001. The role of neuronal and extraneuronal plasma membrane transporters in the inactivation of peripheral catecholamines. Pharmacol. Ther. 91, 35–62.

Esler, M., Jennings, G., Leonard, P., Sacharias, N., Burke, F., Johns, J., Blombery, P., 1984. Contribution of individual organs to total noradrenaline release in humans. Acta Physiol. Scand. Suppl. 527, 11–16.

Esler, M., Jennings, G., Lambert, G., Korner, P., 1987. Local autonomic activity in primary hypertension. In: Hofman, A., Grobee, D.E., Schalekamp, M.A.D.H. (Eds.), The Early Pathogenesis of Primary Hypertension. Excerpta Medica (International Congress Series 737), Amsterdam, pp. 141–155.

Fagius, J., Berne, C., 1994. Increase in muscle nerve sympathetic activity in humans after food intake. Clin. Sci. (London) 86, 159–167.

Ferguson, D.W., Berg, W.J., Sanders, J.S., 1990. Clinical and hemodynamic correlates of sympathetic nerve activity in normal humans and patients with heart failure: evidence from direct microneurographic recordings. J. Am. Coll. Cardiol. 16, 1125–1134.

Grassi, C., Passatore, M., 1988. Action of the sympathetic system on skeletal muscle. Ital. J. Neurol. Sci. 9, 23–28.

Grassi, C., Passatore, M., 1990. Spontaneous sympathetic command to skeletal muscles: functional implications. Funct. Neurol. 5, 227–232.

Grassi, G., Seravalle, G., Cattaneo, B.M., Lanfranchi, A., Vailati, S., Giannattasio, C., Del Bo, A., Sala, C., Bolla, G.B., Pozzi, M., 1995. Sympathetic activation and loss of reflex sympathetic control in mild congestive heart failure. Circulation 92, 3206–3211.

Gronlund, B., Astrup, A., Bie, P., Christensen, N.J., 1991. Noradrenaline release in skeletal muscle and in adipose tissue studied by microdialysis. Clin. Sci. 80, 595–598.

Kiss, J.P., Zsilla, G., Mike, A., Zelles, T., Toth, E., Lajtha, A., Vizi, E.S., 1995. Subtype-specificity of the presynaptic alpha 2-adrenoceptors modulating hippocampal norepinephrine release in rat. Brain Res. 674, 238–244.

Kopin, I.J., 1985. Catecholamine metabolism: basic aspects and clinical significance. Pharmacol. Rev. 37, 333–364.

Lambert, G.W., Kaye, D.M., Vaz, M., Cox, H.S., Turner, A.G., Jennings, G.L., Esler, M.D., 1995. Regional origins of 3-methoxy-4-hydroxyphenylglycol in plasma: effects of chronic sympathetic nervous activation and denervation, and acute reflex sympathetic stimulation. J. Auton. Nerv. Syst. 55, 169–178.

Langeloh, A., Bonisch, H., Trendelenburg, U., 1987. The mechanism of the 3H-noradrenaline releasing effect of various substrates of uptake1: multifactorial induction of outward transport. Naunyn Schmiedebergs Arch. Pharmacol. 336, 602–610.

Lundvall, J., Edfeldt, H., 1994. Very large range of baroreflex sympathetic control of vascular resistance in human skeletal muscle and skin. J. Appl. Physiol. 76, 204–211.

Mundinger, T.O., Boyle, M.R., Taborsky Jr., G.J., 1997. Activation of hepatic sympathetic nerves during hypoxic, hypotensive and glucopenic stress. J. Auton. Nerv. Syst. 63, 153–160.

Nicholls, D.G., 1994. Proteins, Transmitters and Synapses. Blackwell Scientific Publications, Oxford, pp. 32–33.

Shannon, J.R., Flattem, N.L., Jordan, J., Jacob, G., Black, B.K., Biaggioni, I., Blakely, R.D., Robertson, D., 2000. Orthostatic intolerance and tachycardia associated with norepinephrine-transporter deficiency. N. Engl. J. Med. 342, 541–549.

Spraul, M., Anderson, E.A., Bogardus, C., Ravussin, E., 1994. Muscle sympathetic nerve activity in response to glucose ingestion. Impact of plasma insulin and body fat. Diabetes 43, 191–196.

Takauchi, Y., Kitagawa, H., Kawada, T., Akiyama, T., Yamazaki, T., 1997. High-performance liquid chromatographic determination of myocardial interstitial dihydroxyphenylglycol. J. Chromatogr. B: Biomed. Sci. Appl. 693, 218–221.

Takauchi, Y., Yamazaki, T., Akiyama, T., 2000. Tyramine-induced endogeneous noradrenaline efflux from in situ cardiac sympathetic nerve ending in cats. Acta Physiol. Scand. 168, 287–293.

Thompson, L.P., Mohrman, D.E., 1983. Blood flow and oxygen consumption in skeletal muscle during sympathetic stimulation. Am. J. Physiol. 245, H66–H71.

Thompson, J.M., Wallin, B.G., Lambert, G.W., Jennings, G.L., Esler, M.D., 1998. Human muscle sympathetic activity and cardiac catecholamine spillover: no support for augmented sympathetic noradrenaline release by adrenaline co-transmission. Clin. Sci. (London) 94, 383–393.

Trendelenburg, U., Langeloh, A., Bonisch, H., 1987. Mechanism of action of indirectly acting sympathomimetic amines. Blood Vessels 24, 261–270.

Wallin, B.G., Thompson, J.M., Jennings, G.L., Esler, M.D., 1996. Renal noradrenaline spillover correlates with muscle sympathetic activity in humans. J. Physiol. 491, 881–887.

Yamazaki, T., Akiyama, T., 1996. Effects of locally administered desipramine on myocardial interstitial norepinephrine levels. J. Auton. Nerv. Syst. 61, 264–268.

Yamazaki, T., Akiyama, T., Shindo, T., 1995. Routine high-performance liquid chromatographic determination of myocardial interstitial norepinephrine. J. Chromatogr. B: Biomed. Appl. 670, 328–331.

Yamazaki, T., Akiyama, T., Kitagawa, H., Takauchi, Y., Kawada, T., Sunagawa, K., 1997. A new, concise dialysis approach to assessment of cardiac sympathetic nerve terminal abnormalities. Am. J. Physiol. 272, H1182–H1187.

Yamazaki, T., Akiyama, T., Kawada, T., Kitagawa, H., Takauchi, Y., Yahagi, N., Sunagawa, K., 1998. Norepinephrine efflux evoked by potassium chloride in cat sympathetic nerves: dual mechanism of action. Brain Res. 794, 146–150.

Yamazaki, T., Akiyama, T., Kawada, T., 1999. Effects of ouabain on in situ cardiac sympathetic nerve endings. Neurochem. Int. 35, 439–445.

Yamazaki, T., Akiyama, T., Kitagawa, H., Kawada, T., Sunagawa, K., 2001a. Dialysate dihydroxyphenylglycol as a window for in situ axoplasmic norepinephrine disposition. Neurochem. Int. 38, 287–292.

Yamazaki, T., Akiyama, T., Mori, H., 2001b. Effects of nociceptin on cardiac norepinephrine and acetylcholine release evoked by ouabain. Brain Res. 904, 153–156.

Youdim, M.B.H., Finberg, J.P.M., Tipton, K.F., 1988. Monoamine oxidase. In: Trendelenburg, U., Weiner, N. (Eds.), Handbook of Experimental Pharmacology. Catecholamine 1, vol. 90/1. Springer, Berlin, pp. 119–192.

Zimpfer, M., Manders, W.T., Barger, A.C., Vatner, S.F., 1982. Pentobarbital alters compensatory neural and humoral mechanisms in response to hemorrhage. Am. J. Physiol. 243, H713–H721.

Zou, A.P., Cowley Jr., A.W., 1997. Nitric oxide in renal cortex and medulla. An in vivo microdialysis study. Hypertension 29, 194–198.